Stanford Geothermal Program
Interdisciplinary Research in
Engineering and Earth Sciences
STANFORD UNIVERSITY
Stanford, California

SGP-TR-54

EXPLORATORY STUDY ON THE INFLUENCE OF THERMAL STRESSING ON THE STRENGTH AND POROSITY OF GRANITE

By

Rajiv Rana

November 1984

Financial support was provided through the Stanford Geothermal Program under Department of Energy Contract No. DE-AT03-80SF11459 and by the Departnent of Civil Engineering, Stanford University.

ABSTRACT

It has been postulated that the cooling of rock by water circulated in a "hot dry rock" geothermal reservoir will induce tensile thermal stresses in the rock of sufficient magnitude to cause large cracks to form and grow. These cracks may create additional, useful heat transfer and flow areas, thereby prolonging the productive life of a reservoir. This thesis explores, experimentally, the influence of thermal stressing on the strength and porosity of granite samples representative of geothermal rock. It is found that strength is reduced dramatically and porosity increased substantially by tensile thermal stressing. Strength reductions and porosity increases may favor formation and growth of thermal cracks in actual reservoirs by reducing local rock fracture toughness and allowing hydrostatic pore pressure to counteract tectonic compressive stress.

TABLE OF CONTENTS

LIST OF FIGURES

LIST OF TABLES

NOMENCLATURE

English Letter Symbols

A = heat transfer surface area

B = Biot number

C = heat capacity rate

C_p = specific heat

E = Young's modulus

h = heat transfer coefficient

K_s = thermal conductivity

L = length of the specimen

p = dimensionless stress

P = tensile strength

q = surface tensile stress

t = time

T = temperature

V = volume of specimen

W = weight of specimen

X = distance below surface

X = dimensionless length, x/L

Greek Letter Symbols

α = coefficient of thermal expansion

ρ = density

ν = Poisson's ratio

β = thermal diffusivity

ζ = Fourier number

Θ = dimensionless temperature

σ = stress

ϕ = porosity

μ = shear modulus

Subscripts

o = initial conditions

∞ = fluid conditions

Superscript

$-$ = average value of the variable

1. INTRODUCTION

The increasing energy problem during recent years has resulted in a greater awareness of alternate energy sources, prominent among which are the substantial subterranean reservoirs of geothermal energy. For several decades, significant quantities of energy have been extracted from natural hydrothermal reservoirs containing either steam or hot water (such as in Ladero, Italy; Wairakei, New Zealand and at The Geysers in northern California). However, much larger amounts of untapped geothermal energy exist at accessible depths in heated rock formations which either contain little water or have permeabilities so low that any existing water cannot be extracted at useful rates. Such "hot, dry rock" (HDR) geothermal reservoirs contain roughly 5×10^4 Quads of accessible energy by U.S. Geological Survey estimate (1), which is about 700 times the total U.S. energy consumption in 1970. Even if efficiences of conversion to electrical energy prove to be only a few percent, development of commercially feasible means for "mining" that energy would still provide a significant, environmentally attractive contribution to U.S. energy resources.

The Los Alamos Scientific Laboratory (LASL) has been testing a concept for extraction of HDR energy that has already demonstrated technical feasibility. Briefly, the concept consists of drilling and casing a well to a depth where rock temperature is sufficiently high (200-400°C), then pressurizing the well, causing a hydraulic fracture to form at the bottom of the wellbore, as depicted in Figure 1.1. The fracture resembles a thin, penny-shaped crack with a width of several millimeters and "radius" of roughly 100 meters. A second well is directionally drilled to intersect the fracture. By pumping water down one

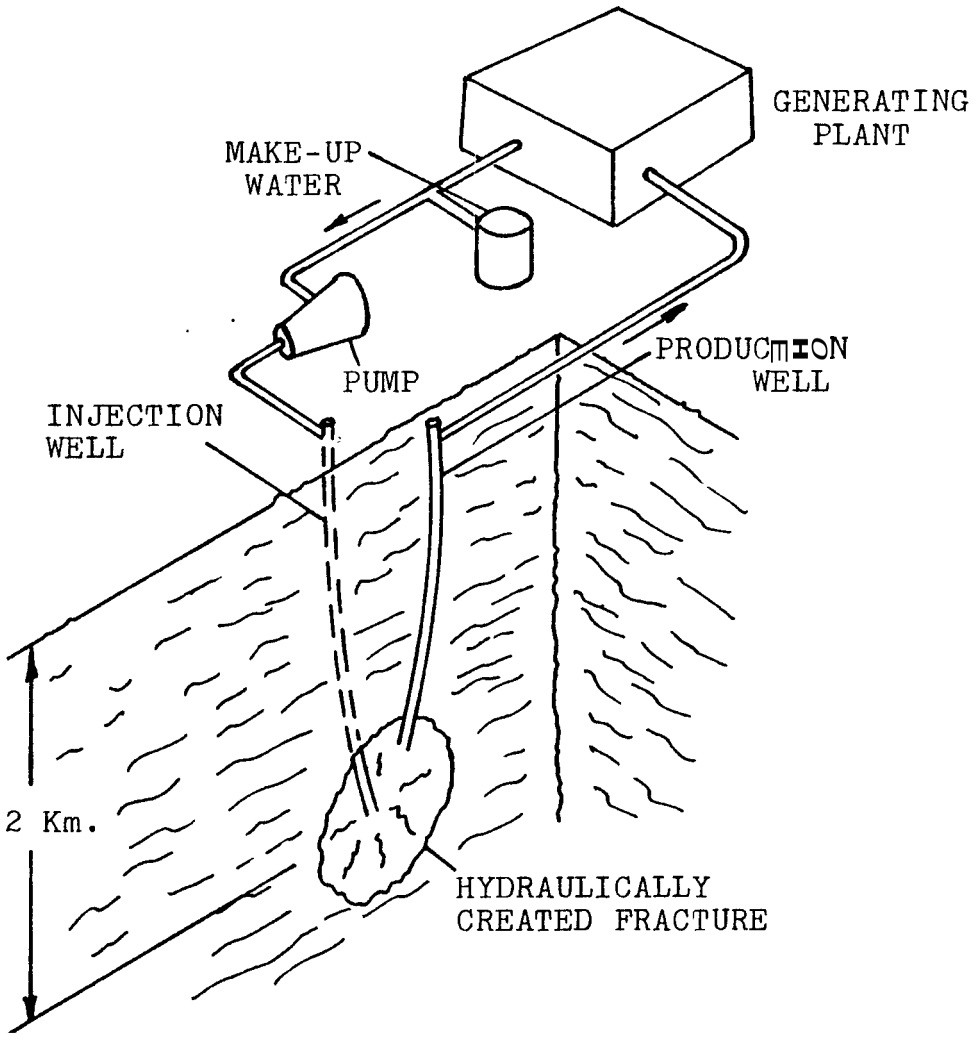

FIG. 1.1 Schematic of Los Alamos Scientific Lab
Hot Dry Rock Geothermal Energy Extraction Scheme

well, circulating it through the fracture, and returning it through the other well, useful energy can be extracted from this underground boiler.

The energy which can be produced from an HDR reservoir is degraded as the rock surrounding the hydraulic fracture is cooled. When the rock temperature is drawn down low enough (≈150°C), economic production of electrical energy may become marginal. Thermal energy recharge from the molten magma kilometers below the fracture takes thousands of years. Recharge from adjoining rock is also a very slow process. Thus the economic viability of HDR energy is yet to be demonstrated in terms of length of production time needed to justify the capital investment in drilling wells, building a generating plant, etc.

Recently it has been suggested (2) that the cooling of the rock surrounding the hydraulic fracture will induce thermal stresses of sufficient magnitude to cause cracks to form and grow perpendicular to the fracture. If these cracks are effective in creating fresh, useable heat transfer and flow areas, then additional energy can be extracted at little additional cost. Furthermore, as a reservoir is drawn down, the decline in rock temperature may be offset by the additional heat transfer area, perhaps leading to relatively stable production temperatures. The extent to which thermal fracturing can increase reservoir output or lengthen useful production time may well have a significant bearing on the commercial feasibility of HDR goethermal energy.

Murphy (2) has proposed that cracks will form and grow with time in those regions where the tensile thermal stress exceeds the sum of the compressive tectonic stress acting perpendicular to the direction of crack growth plus the rock tensile strength. This criterion assumes impermeable rock. He noted, however, that if the rock has sufficient

permeability to allow water infiltration such that the rock pore pressure is raised to hydrostatic levels, then the effective compressive stress to be overcome will be greatly reduced, increasing the propensity for and rate of thermal fracturing. Murphy also estimated that if thermal cracks grow to the point where their aperture is on the order of 0.5 mm, significant flowrates and heat transfer can be expected. An analytical study by Nemat-Nasser et al. (3, 4) indicates that thermal cracks forming perpendicular to the hydraulic fracture will initially have a spacing roughly equal to their depth. With time, some of the cracks will continue to propagate to maintain the approximate equality between their depth and spacing, while the others will be arrested. Later, secondary thermal cracks may form perpendicular to the original thermal cracks, leading to a three-dimensional fracture network.

The thermal stresses induced by cooling water may also change the physical properties of the rock, but little is known about this. These changes may, in turn, influence HDR thermal cracking behavior. In a preliminary effort to see if such changes occur and are likely to be significant, this thesis explores experimentally the effect of thermal stressing on the strength and porosity of granite block typical of that found in HDR reservoirs.

2. LITERATURE REVIEW

The behavior of brittle materials subjected to thermal stressing has been studied by a number of researchers. The literature survey in this section reviews work undertaken to investigate material properties which influence the thermal stress resistance of a brittle substance.

Winkelman and Schott (5) considered a semi-infinite body, originally at zero degree temperature throughout, suddenly cooled to a given temperature along the free surface. The material's thermal shock resistance, defined by the ratio of the material's tensile strength, P, to the applied surface (maximum) tensile stress, q, was given by:

$$P/q = P/\{\sqrt{k_s}/[E\alpha(\rho C)^{1}/2(\Delta T)\}(1/B) \qquad (2.1)$$

where

k_s = thermal conductivity

E = Young's Modulus

α = coefficient of thermal expansion

ρ = density

C = heat capacity rate

B = Biot number = $\frac{hL}{k_s}$

h = heat transfer coefficient at surface

L = test specimen thickness

AT = Initial temperature difference between the specimen and quenching medium.

The authors postulated that thermal failure will not occur so long as (P/q) >1, and found that Equation 2.1 predicted quite reasonably the

maximum surface temperature drop the material could withstand without failing in tension. Experiments were done with 1 cm and 2 cm cubes made of twenty different types of glass. Smaller cubes consistently withstood greater temperature differences than larger ones.

Lidman & Bobrowsky (6) investigated the mechanism of fracture in ceramic gas-turbine blades brought about by thermal shock due to unsteady heat flows. Thermal shock resistance was expressed as the ratio:

$$P/q = 2k_s P/(\alpha E h \Delta T) \qquad (2.2)$$

where α, k_s, E, h, and AT are as defined in Eq. (2.1)

In terms of material properties, the coefficient of thermal shock resistance, S, can be written as $S = k_s P/E\alpha$. It was shown experimentally that the larger the S value, the greater the surface temperature difference the material could resist without fracturing.

The case of a flat circular plate, unrestrained at its edges and rapidly cooled or heated, was examined by Cheng (7). Both symmetric and nonsymmetric heat transfer cases were considered. Experiments were done on 2 in diameter x 1/4 in thick disks made of ceramic and ceramal materials. The experiments consisted of uniformly heating the specimen 'on both sides in a furnace to 1800°F and subsequently cooling them in an air stream of 60°F. The thermal shock resistance was given by:

$$\frac{P}{q} = P/[p^*(\alpha E \Delta T)/(1-\nu)] = \left[\frac{P(1-\nu)}{\alpha E \Delta T}\right] 1 \left[\frac{1}{p^*}\right] \qquad (2.3)$$

where

p^* = maximum value of the dimensionless stress = $\frac{\sigma(1-\nu)}{\alpha E \Delta T}$

In Eqs. 2.1 and *2.2,* q is per unit length as per Ref. 6.

σ = thermal stress at any point in the disc

ν = Poisson's ratio.

Experiments showed that no specimen with a (P/q) value of less than unity survived a single complete shock, whereas each with a (P/q) in excess of unity withstood at least 25 cycles. Cheng also noted that thermal stock resistance is not an intrinsic property of a material but greatly depends on the manner in which the heat is supplied (i.e., on h) and on the form and dimension of the specimen tested.

More work was done on 2 in diameter x 1/4 in disks by Mason & Smith (8). They used stealite and glass specimens and rather than cooling the flat lateral faces in the manner of Cheng, they insulated these and subjected the discs to quenching along the free periphery. The authors noted that the thermal shock resistance of most brittle materials is a function of two or more parameters. The relative importance of each parameter depends on the severity of the quench for a given size specimen of a given material. They found that for materials obeying the maximum stress theory of failure, the parameter governing thermal shock resistance is $P/(E\alpha)$ only for very severe quenches (large h) or very large characteristic dimensions. The thermal conductivity, k_s, has little influence under these conditions, even though it becomes important for relatively small values of Biot number where heat transfer rate is largely governed by the value of thermal conductivity. Thus thermal shock resistance cannot, in general, be expressed by a single parameter, such as $k_s P/E\alpha$, as often has been attempted. Instead, two or more parameters must be evaluated depending upon the conditions of test geometry and quench severity. The authors also examined their experimental results in terms

of Weibull's statistical theory of strength. This theory is based on the assumed presence of flaws and states that the probability of failure of a given specimen depends on the volume under stress and on the stress distribution. They calculated the maximum risk of rupture, a criterion for onset of thermal stress cracking, for the circular discs. Then they evaluated the stress distribution for instants when the risks of rupture were a maximum. Comparison with stress distributions at the time of maximum stress showed that the stress distribution based on Weibull's theory gave a better estimation of failure in the circular discs considered.

Another thorough analytical study of the thermal shock resistance phenomenon was undertaken by Mervoelli, et. al. (9). They also experimented with thin circular disks (measuring 2 1/8 in dia. x 1/4 in thick), the lateral surfaces of which were assumed to be perfectly insulated so that heat conduction was constrained to the radial direction alone. They chose rock specimens, especially basalt, quartzite and taconite. Two cases of failure were considered, one predicted by the maximum stress theory and one similar to Weibull's theory, referred to as the "average stress theory". Cooling experiments showed that there was little difference between the predictions of failure by both theories when the Biot number was small (under mild quenching). Significant differences were found when the Biot number was large (under severe quenching), in which case failures correlated better with the average stress theory.

Hasselman (10, 11) discussed the principal material properties which affect the propagation of cracks under conditions of thermal shock. From these material properties, "thermal shock damage resistance parameters" were derived, which are indicative of the relative resistance of materials

to damage after cracking by thermal shock has been nucleated. The author applied Griffith's criterion for crack propagation, and concluded that for a low degree of damage there must be small values of strength and high values of Young's modulus of elasticity and Poisson's ratio. Moreover the extent of crack propagation was found to be a function of specimen volume, numbers of cracks nucleated, etc. The author also noted that microstructural inhomogeneities in the material act as micromechanical thermal stress concentrators, helping to nucleate cracks but reducing subsequent crack propagation.

Crack propagation was further analyzed by Hasselman (12). Thermal shock experiments on circular aluminum oxide rods showed that an initially short crack, unstable at a critical temperature difference, propagates to a new length such that a finite increase in temperature difference is required before the crack will continue to propagate. The author drew an analogy between crack propagation under thermal shock and under constant deformation (strain).

Further study of the severity of thermal shock required to initiate cracking and the amount of cracking produced by a shock of fixed severity was done by Davidge and Tappin (13). Experiments utilized ceramic Al_2O_3 specimens of both square and round cross-sections which were quenched in 20°C water. The fracture strength was determined by three point bend tests on quenched and unquenched specimens and showed a drastic reduction for specimen temperatures of 220°C. The amount of cracking was related to U/γ_F, where U is the elastic energy produced by the shock and γ_F is the effective surface energy. The author found that quantity U/γ_F seemed to define the limit of new crack area produced.

The effect of porosity on thermal stress fracture has been studied by various authors (14-18). This effect can be investigated from the points

of view of both nucleation of cracking and degree of damage. Coble and Kingerly (14) demonstrated for sintered alumina that the overall effect is to lower thermal shock crack nucleation resistance. From the point of view of crack propagation, however, the effect of porosity on strength and on Young's modulus of elasticity is to reduce substantially the elastic energy stored at fracture. Porosity, therefore, tends to reduce the degree of damage in agreement with the observations of Parmelee and Westman (15), Bartsch (16), Kato and Okuda (17), and Richardson (18). Pores are often cited as acting as crack arrestors, and in this manner are thought to increase thermal shock damage resistance.

Gupta (19) demonstrated the effect of microstructure, especially of grain size, on the strength degradation characteristics of alumina subjected to thermal shock. High density aluminas with grain sizes of 10, 28, 34, 40, and 80 μm were subjected to thermal shock and then tested for strength in four point bending tests. These experiments showed that the strength degradation was catastrophic for all specimens except those with a grain size of 80 μm. The author points out that above a critical grain size the failure characteristic becomes completely "noncatastrophic". Formation of microcracks in the highly stressed zone ahead of the major propagating crack results in slow crack growth and hence the "noncatastrophic" failure. A recent study (20) on mica glass-ceramic under thermal shock also indicated that when grain size is increased from 70 to 200 μm, the failure mode changes from catastrophic to "noncatastrophic".

From the above brief review, it is clear that the cracking of brittle material due to thermal stressing can, in general, be a function of several variables, including mechanical properties, thermal properties, specimen size and shape, severity of the thermal shock and microstructura

characteristics (e.g., grain size). The two most popular failure theories for crack nucleation are the maximum stress theory (in which cracking is postulated when the tensile strength is exceeded at the point of maximum stress) and the average stress theory (in which cracking is expected when stress averaged over a critical volume of material exceeds the tensile strength).

3. EXPERIMENTAL PROCEDURE

3.1 Apparatus to Produce Thermal Stress

In order to investigate the influence of thermal stressing on granite strength and porosity, the experimental setup shown schematically in Figure 3.1 was devised. It consists of a heating oven (A), temperature controller (B), temperature recorder (C), and water quenching system (D). The heating system is a Kress Kiln (C-11-H) with inner dimensions of 11" x 11" x 11" and a power rating of 15 amps at 110 volts. Heating elements are installed around the four sides to promote uniform heating. A metal sheet is put just in front of the heaters to further increase the uniformity. Temperature inside the kiln is governed by the time proportioning temperature controller (B). Desired heating rates can be achieved by a proper combination of power regulators and the temperature controller.

Initially, a 5" x 5" x 5" granite block, shown in Figure 3.2, was used for the first few thermal shock experiments. The block was heated in the oven at a rate of 2°F/min to avoid thermal cracking during heating. The uniformity of temperature distribution inside the rock was checked by measuring temperatures at ten different locations shown in Figure 3.2. One inch deep holes were drilled at these locations and thermocouples installed using Saueriesen Low Expansion cement to provide good contact with the rock. This cement is a very good conductor thus ensuring a good temperature response. Deeper holes were not possible due to the difficulties encountered in attempting to drill them with available equipment. The thermocouples used were J-type and were calibrated with boiling water before and after the experiments. During heating, temperatures recorded at locations 4, 9, 10 were within ± 1°F of each other, showing uniform heating of the block. Also the temperatures at 6, 7, 8 were

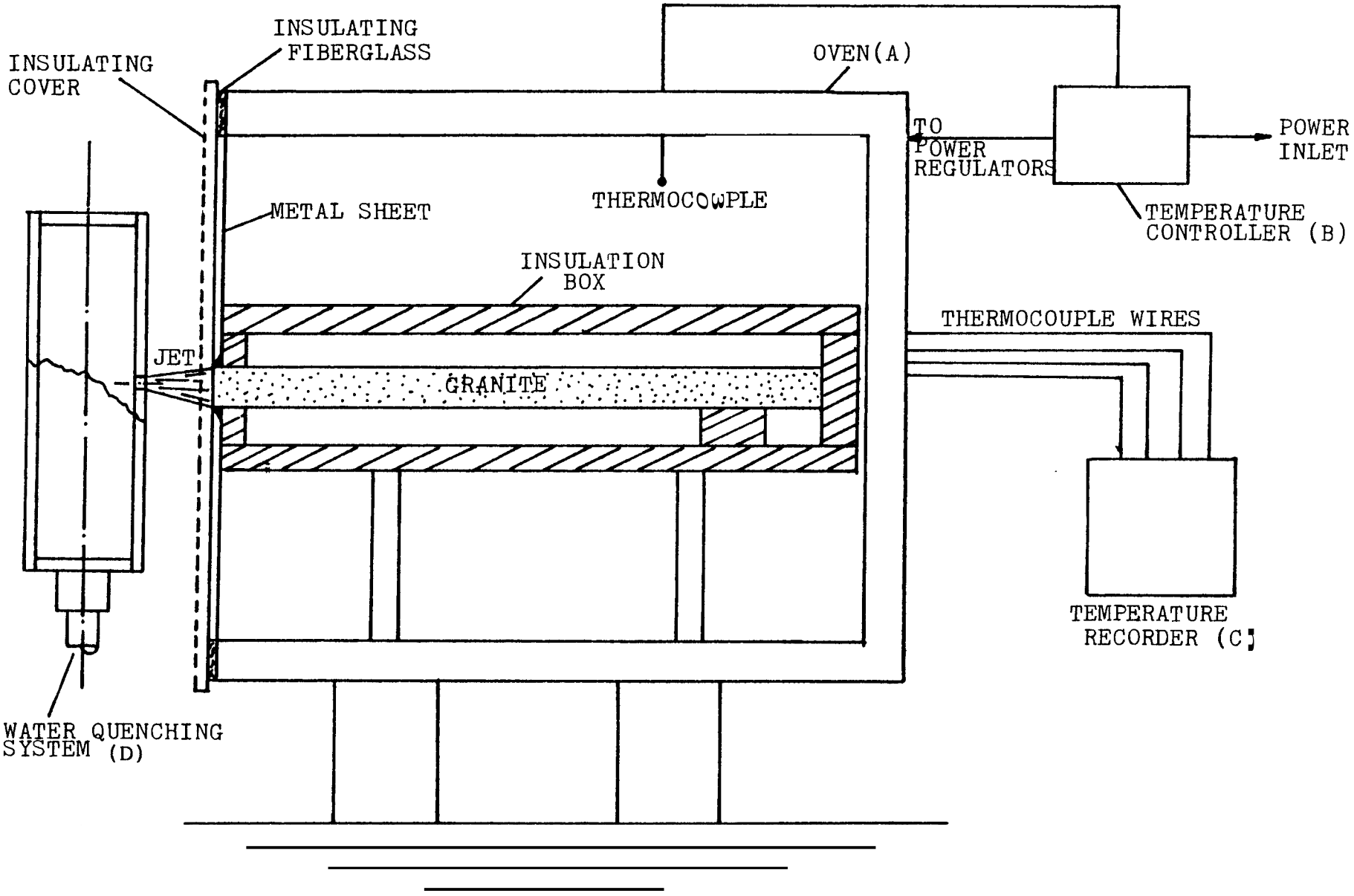

FIG.3.1 Experimental Setup for Producing Thermal Stress

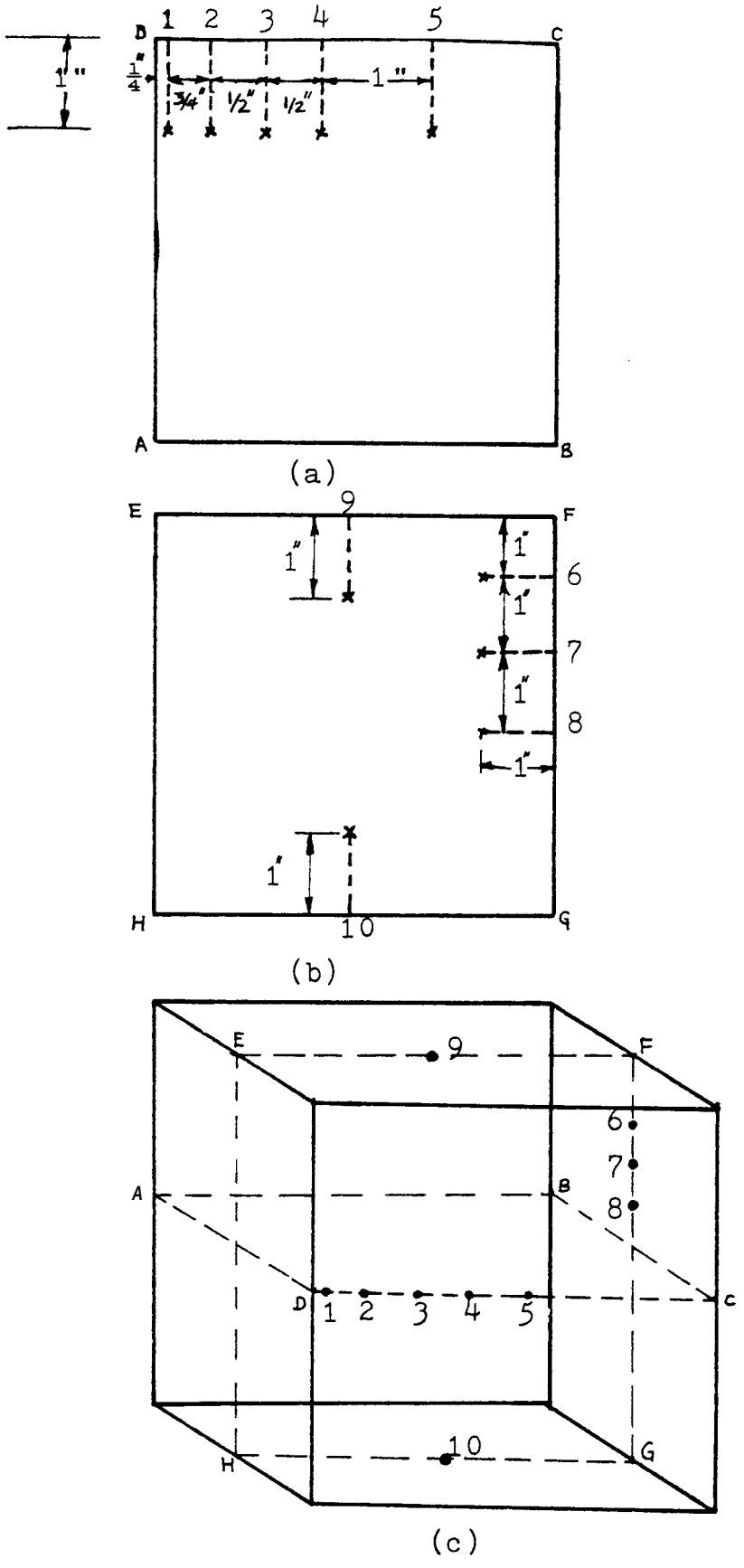

FIG. 3.2 Granite Block with Dimensions 5"x5"x5" and The Thermocouple Arrangement

within ±2°F. The spatial variation of temperature was about 5°F. Temperatures were recorded continuously while quenching the block for approximately an hour. During quenching, the temperature at 3 showed a sudden drop after eighteen minutes. he thermocouple at 3 showed no malfunctioning when checked after the experiment. Another quenching run showed a sudden change in temperature at location 5 though the thermocouple showed no malfunctioning. An explanation for the malfunctions was not apparent.

To simplify calculations of transient temperature and thermal stress behavior, all subsequent experiments utilized thin slabs to better approximate one-dimensional heat flow. The details of the specimen and method of insulation are shown in Figure 3.3. The granite slabs (2-1/4" x 10" x 1/4") were cut from a larger block with a 1/16 in thick diamond saw. Asbestos was used for building the insulation box and was made air tight with Saueriesen cement. The air gap in the box provided even better insulation.

3.2 Temperature Distribution in Specimens

The first task in calculating the thermal stress distribution within the rock is the determination of temperature distribution in it. Heat transfer in the granite block specimens can be analyzed approximately by considering a solid of infinite thickness as shown in Figure 3.4. The solid is initially at the temperature T_0 throughout, and the surface is cooled convectively by the flowing fluid at temperature T_∞. All the heat flow is assumed to be only in the direction normal to the slab, denoted by the x coordinate. It is also assumed that the temperature variation within he slab depends only on the conditions imposed at the x = 0 surface.

The assumptions made to simplify the heat transfer analysis are: (i) thermal conductivity, k_s, specific heat, C_p, and density, ρ, of the rock are

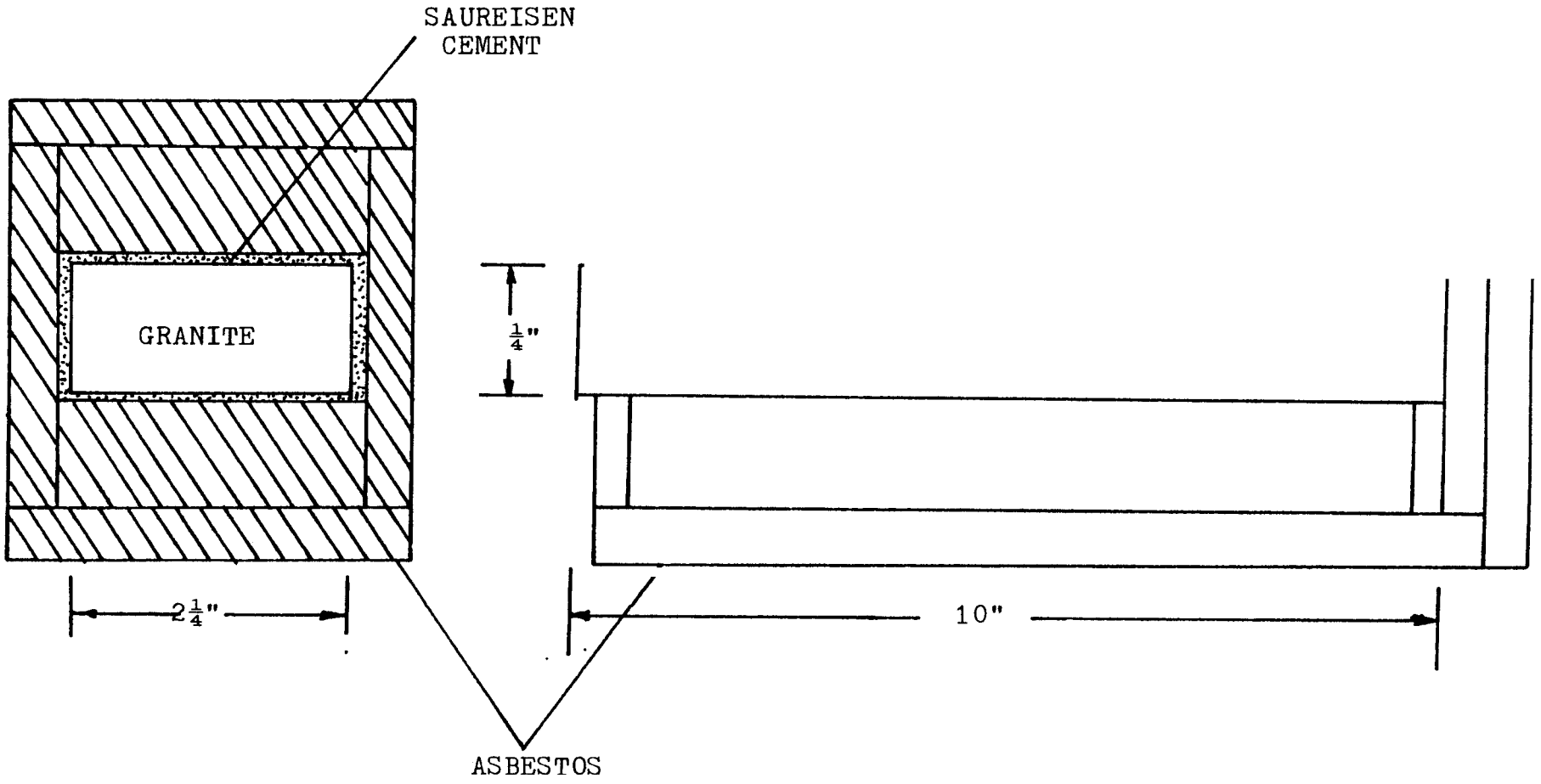

FIG. 3.3 Smaller Granite Specimen and Insulation System

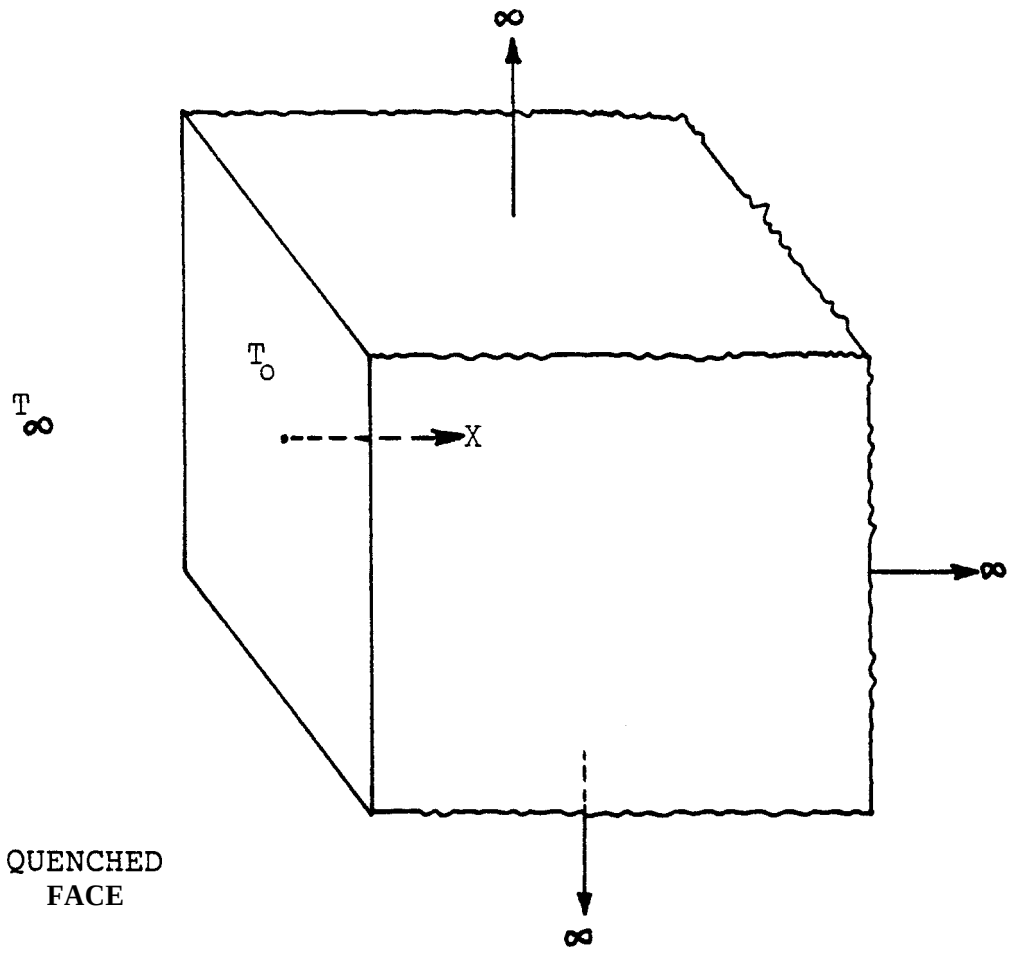

FIG. 3.4 Semi-Infinite Solid

assumed constant with respect to temperature and (ii) the surface heat transfer coefficient, h, is also assumed to be constant.

The one-dimensional, nonsteady heat transfer for a semi-infinite solid is governed by the conduction equation

$$\beta \frac{\partial^2 T}{\partial x^2} = \frac{\partial T}{\partial t} \qquad \text{where:} \quad \beta = \frac{k_s}{\rho C_p} \tag{3.1}$$

The initial and boundary conditions for the rock fluid system are at

$$t = 0 \; : \; T = T_o \quad \text{for } x \geq 0 \tag{3.2a}$$

where: t = time

x = distance below the surface

T = temperature of the solid at time t

T_o = initial temperature of the solid

$$\text{at } t > o \; : \; \bar{h}A[T_\infty - T(o,t)] = k_s A\left(\frac{\partial T}{\partial x}\right)_{x=o} \tag{3.2b}$$

where T_∞ = fluid temperature

$\bar{h}$ = average surface heat transfer coefficient

A = heat transfer surface area

The solution, obtained by the method of Laplace transforms [22], is given by:

$$\frac{T(x,t)-T_o}{T_\infty - T_o} = 1-\text{erf}\sqrt{\frac{x^2}{4\beta t}} + \left[\exp\left(\frac{\bar{h}x}{k_s} + \frac{\bar{h}^2\beta t}{k_s^2}\right)\right] \cdot \left[1-\text{erf}\left(\sqrt{\frac{x^2}{4\beta t}} + \sqrt{\frac{\bar{h}^2\beta t}{k_s^2}}\right)\right] \tag{3.3}$$

The term "erf" in Eq. (3.3) is the error function and is given by:

$$\text{erf}\left(\sqrt{\frac{x^2}{4\beta t}}\right) = \frac{2}{\sqrt{\pi}} \int_o^{\sqrt{\frac{x^2}{4\beta t}}} e^{-\lambda^2} d\lambda \tag{3.4}$$

Values of the error function are usually tabulated in standard mathematical handbooks. The computer program developed here for determining the temperature profile uses IBM's standard mathematical error function (Appendix). The heat transfer conditions described by Equation 3.3 are also realized in a finite slab of thickness L which is insulated around its periphery (Fig. 3.5). The initial and boundary conditions given by Equation 3.2 are also valid for this slab. As long as the temperature effect has not significantly reached the face x = L, the semi-infinite solution is still applicable.

The solution for the finite slab of length L, which more closely approximates the situation in the granite block specimen, can be expressed in dimensionless form by defining the following parameters:

$X = \frac{x}{L}$

B = Biot Number = hL/k_s

ζ = Fourier Number = $h^2\beta t/k_s^2$

Θ = dimensionless temperature = $(T-T_\infty) \div (T_o-T_\infty)$

Using the above parameters, Equation 3.3 becomes

$$\Theta = \text{erf}(X\ D) + [\exp\ (BX + \zeta)]\ .\ [1-\text{erf}(X\ D + \sqrt{\zeta})] \qquad (3.5)$$

where $D = \sqrt{L^2/4\beta t}$.

Using representative values of ρ, C_p and k_s for granite, the temperature-time distributions for h = 5.0 and h = 300.0 Btu/hr F. ft^2 are plotted in Figures 3.6 and 3.7. As expected, the effect of temperature disturbance is felt more rapidly at the face X = 1.0 for h = 300.0 than

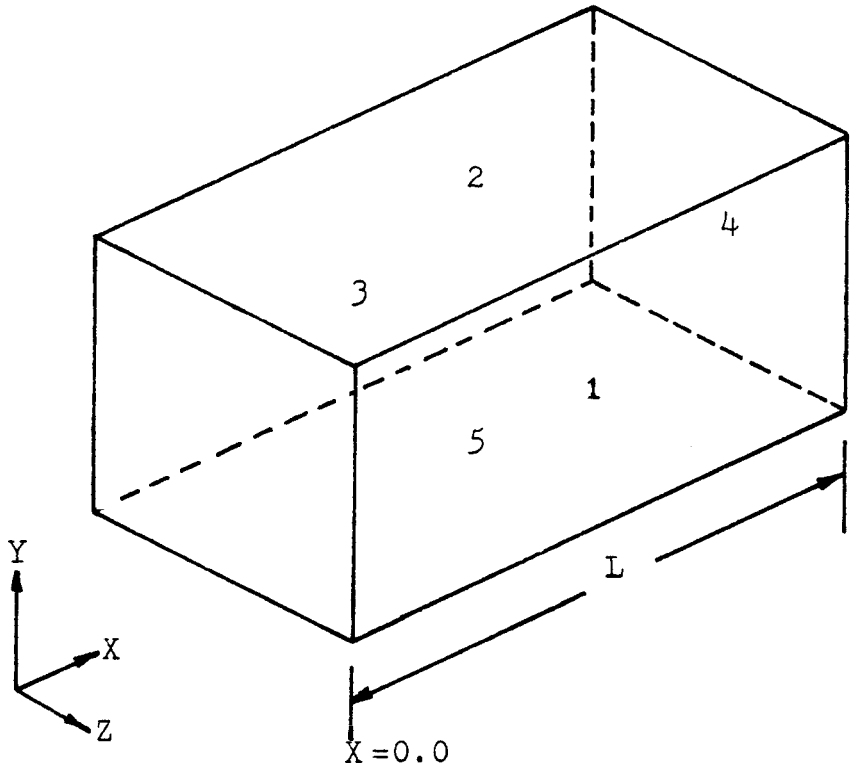

Insulated Faces: 1,2,3,4,5

FIG. *3.5* Finite Solid Insulated Except at Face X=0

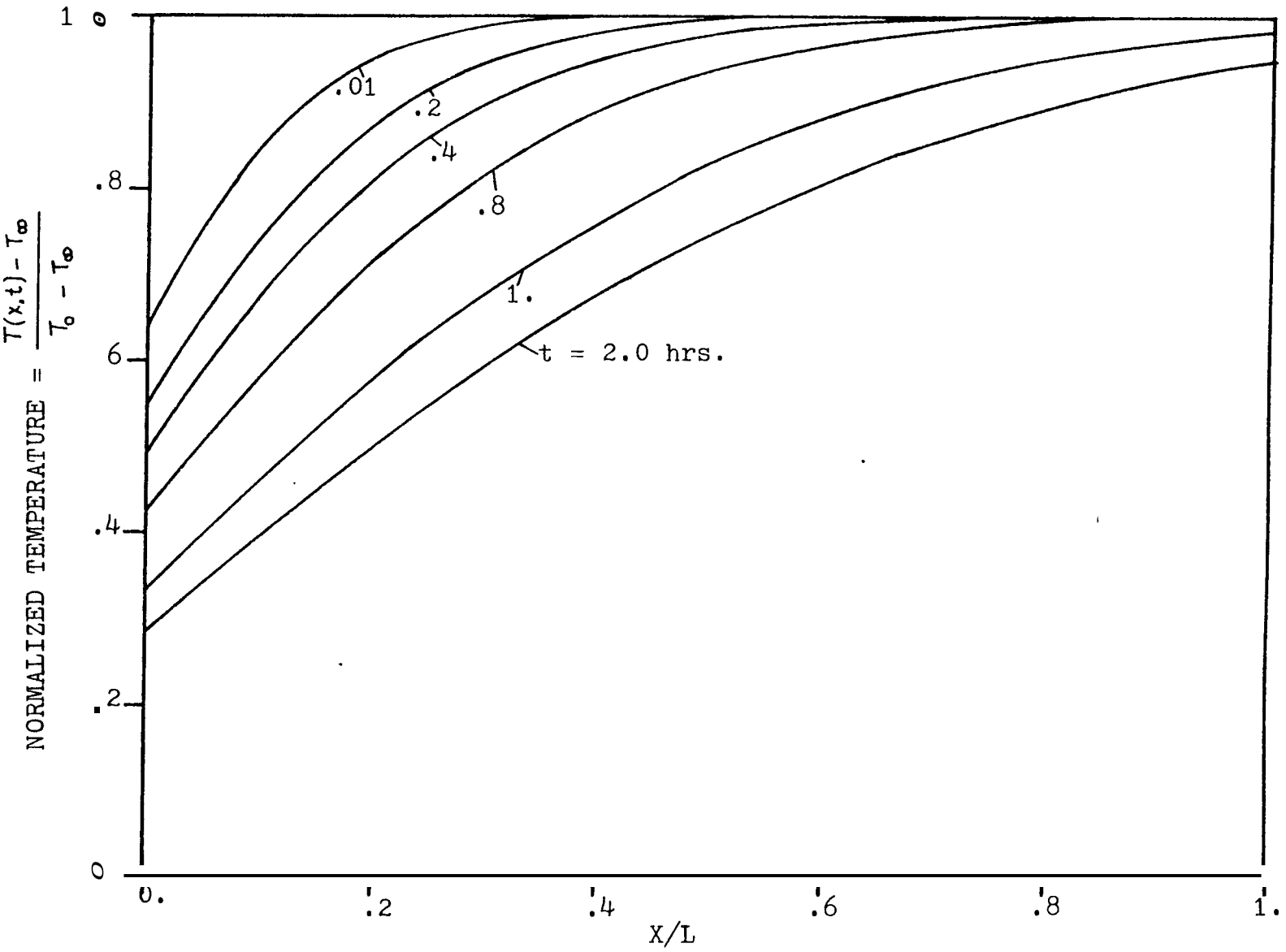

FIG. 3.6 Estimated Temperature Distribution in Granite Block for h = 5 Btu/hr ft^2 °F

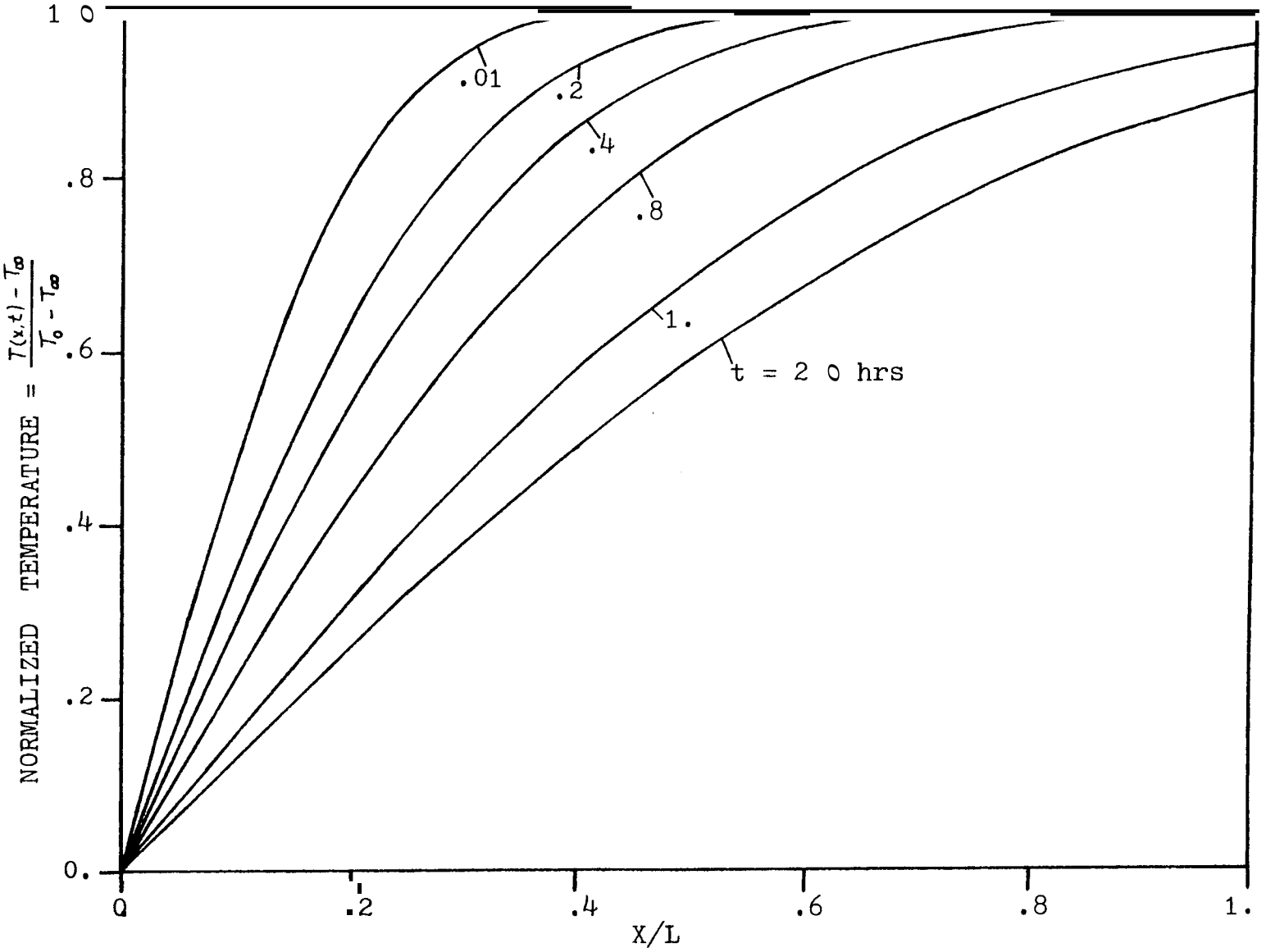

FIG 3.7 Estimated Temperature Distribution in Granite Block for h = 300 Btu/hr ft^2 °F

for h = 5.0. If applicability of the infinite slab solution is defined by the condition: $T_{X=1.0}/T_o \geq 0.95$, then from Figures 3.6 and 3.7, applicability is achieved for $t \leq 1$ hrs for the case of h = 300.00 and $t \leq 2$ hrs for h = 5.0. This provides an estimate of the time duration during which a finite slab of length L can be cooled and still be considered an infinite solid.

3.3 Thermal Stress Distribution:

After the temperature-time distribution is found, one can proceed to calculate the stress distributions inside the solid. In order to simplify the analysis, the following idealizations are made:

(i) The hard, crystalline rock is treated as a linearly elastic, isotropic, homogeneous, brittle continuous medium.

(ii) The rock is assumed to have temperature independent thermal and mechanical properties.

(iii) Coupling between thermal and elastic behavior, as well as inertial effects, are negligible.

(iv) Body forces are considered to be negligible as compared to thermal stresses.

The governing thermoelastic equations to be satisfied are equations of equilibrium, equations of compatibility and the boundary conditions. The equations of equilibrium expressed in terms of stress components for zero body forces are written in Cartesian coordinates as follows:

$$\frac{\partial \sigma_{xx}}{\partial x} + \frac{\partial \sigma_{xy}}{\partial y} + \frac{\partial \sigma_{xz}}{\partial z} = 0$$

$$\frac{\partial \sigma_{xy}}{\partial x} + \frac{\partial \sigma_{yy}}{\partial y} + \frac{\partial \sigma_{yz}}{\partial z} = 0$$

$$\frac{\partial \sigma_{xz}}{\partial x} + \frac{\partial \sigma_{yz}}{\partial y} \quad \frac{\partial \sigma_{zz}}{\partial z} = 0 \qquad (3.6)$$

The compatibility equations in terms of stress components are:

$$(1+\nu)\nabla^2\sigma_{xx} + \frac{\partial^2 H}{\partial x^2} + \alpha E \left(\frac{1+\nu}{1-\nu}\nabla^2 T + \frac{\partial^2 T}{\partial x^2}\right) = 0$$

$$(1+\nu)\nabla^2\sigma_{yy} + \frac{\partial^2 H}{\partial y^2} + \alpha E \left(\frac{1+\nu}{1-\nu}\nabla^2 T + \frac{\partial^2 T}{\partial y^2}\right) = 0$$

$$(1+\nu)\nabla^2\sigma_{zz} + \frac{\partial^2 H}{\partial z^2} + \alpha E \left(\frac{1+\nu}{1-\nu}\nabla^2 T + \frac{\partial^2 T}{\partial z^2}\right) = 0$$

$$(1+\nu)\nabla^2\sigma_{xz} + \frac{\partial^2 H}{\partial x \partial z} + \alpha E \left(\frac{\partial^2 T}{\partial z \partial x}\right) = 0$$

$$(1+\nu)\nabla^2\sigma_{yx} + \frac{\partial^2 H}{\partial y \partial x} + \alpha E \left(\frac{\partial^2 T}{\partial y \partial x}\right) = 0$$

$$(1+\nu)\nabla^2\sigma_{yz} + \frac{\partial^2 H}{\partial y \partial z} + \alpha E \left(\frac{\partial^2 T}{\partial y \partial z}\right) = 0 \qquad (3.7)$$

where

$$H = \sigma_{xx} + \sigma_{yy} + \sigma_{zz}$$

and $$\nabla^2 = \frac{\partial^2}{\partial x^2} + \frac{\partial^2}{\partial y^2} + \frac{\partial^2}{\partial z^2}$$

The semi-infinite solid under consideration has all the surfaces free of tractions. In this case the boundary conditions are

$$\sigma_{xx}n_x + \sigma_{xy}n_y + \sigma_{xz}n_z = 0$$

$$\sigma_{xy}n_x + \sigma_{YY}n_Y + \sigma_{yz}n_z = 0$$

$$\sigma_{xz}n_x + \sigma_{yz}n_y + \sigma_{zz}n_z = 0 \qquad (3.8)$$

where: n_x, n_y, n_z are unit normals in the x, y, and z directions, respectively.

Now we seek a stress distribution which satisfies Equations 3.6, 3.7, and 3.8. Since the temperature variation is only considered to be in the direction of x, that is T = T(X), it is reasonable to assume [21] that the stress components will be of the form

$$\sigma_{YY} = \sigma_{zz} = f(x)$$

$$\sigma_{xx} = \sigma_{xz} = \sigma_{yz} = \sigma_{xy} = 0 \qquad (3.9)$$

Direct substitution shows that the equilibrium equations are satisfied for the stress components described by Equation 3.9. Of the six equations of compatibility, the last three are satisfied and the first three will be satisfied provided that

$$\frac{d^2}{dx^2}\left\{f(x) + \frac{\alpha E}{1-\nu} T\right\} = 0$$

The form of the non-zero stress components is then:

$$\sigma_{YY} = \sigma_{zz} = f(x) = -\frac{\alpha E}{1-\nu} T + C_1 + C_2 X$$

where the constants C_1 and C_2 are to be determined from the boundary conditions of zero tractions on the edges of the solid. From the form of this result, however, the tractions cannot be made zero throughout the length of the solid. It is possible, however, to choose the constants C_1 and C_2 such that for any temperature T(X), the resultant forces and moments (per unit length) produced by σ_{YY} and σ_{zz} are zero over the edges of the solid, that is,

$$\int_0^L \sigma_{yy} dx = \int_0^L \sigma_{yy}\, x\, dx = 0 \qquad (3.11)$$

and similarly for σ_{zz}. Constants C_1 and C_2 evaluated using the above conditions are

$$C_1 = \left[\frac{4}{L}\int_0^L T dx - \frac{-}{L^2}\int_0 T x dx\right] \cdot \frac{\alpha E}{1-\nu}$$

$$C_2 = \left[\frac{12}{L^3}\int_0^L T x dx - \frac{}{L^2}\int_0 T dx\right] \cdot \frac{\alpha E}{1-\nu} \qquad (3.12)$$

Thus the solution for thermal stress becomes

$$\sigma_{YY} = \sigma_{zz} = \left(\frac{\alpha E}{1-\nu}\right) \left[-T + \frac{2}{L}(2L - 3x)\int_0^L T dx + \frac{6}{L^3}(2L - x)\int_0^L T x dx\right] \qquad (3.13)$$

Substituting the temperature profile given by Equation 3.5 into 3.13, the stress due to quenching for the slab under consideration becomes

$$\sigma^* = \frac{\sigma(1-\nu)}{\alpha E} = [-\Theta + (4 - 6X)\int_0^1 \Theta dX + 6(2X - 1)\int_0^1 \Theta X dX] \qquad (3.14)$$

The integrals in Equation 3.14 were evaluated using Simpson's rule (Appendix). The thermal stresses (in dimensionless form) are graphically presented in Figures 3.8 through 3.13. Positive stresses are tensile and negative ones compressive. The stress is plotted for various times. Two cases of surface heat transfer rate are considered, namely h = 5.0 and h = 300.0 Btu/hr F. ft^2. As can be seen, thermal stresses are tensile at and near the surface being quenched and become compressive on the interior. Also, the stresses are tensile at and near the end face, i.e., at X = 1.0. Maximum stresses develop at the face X = 0. Comparison of the two cases

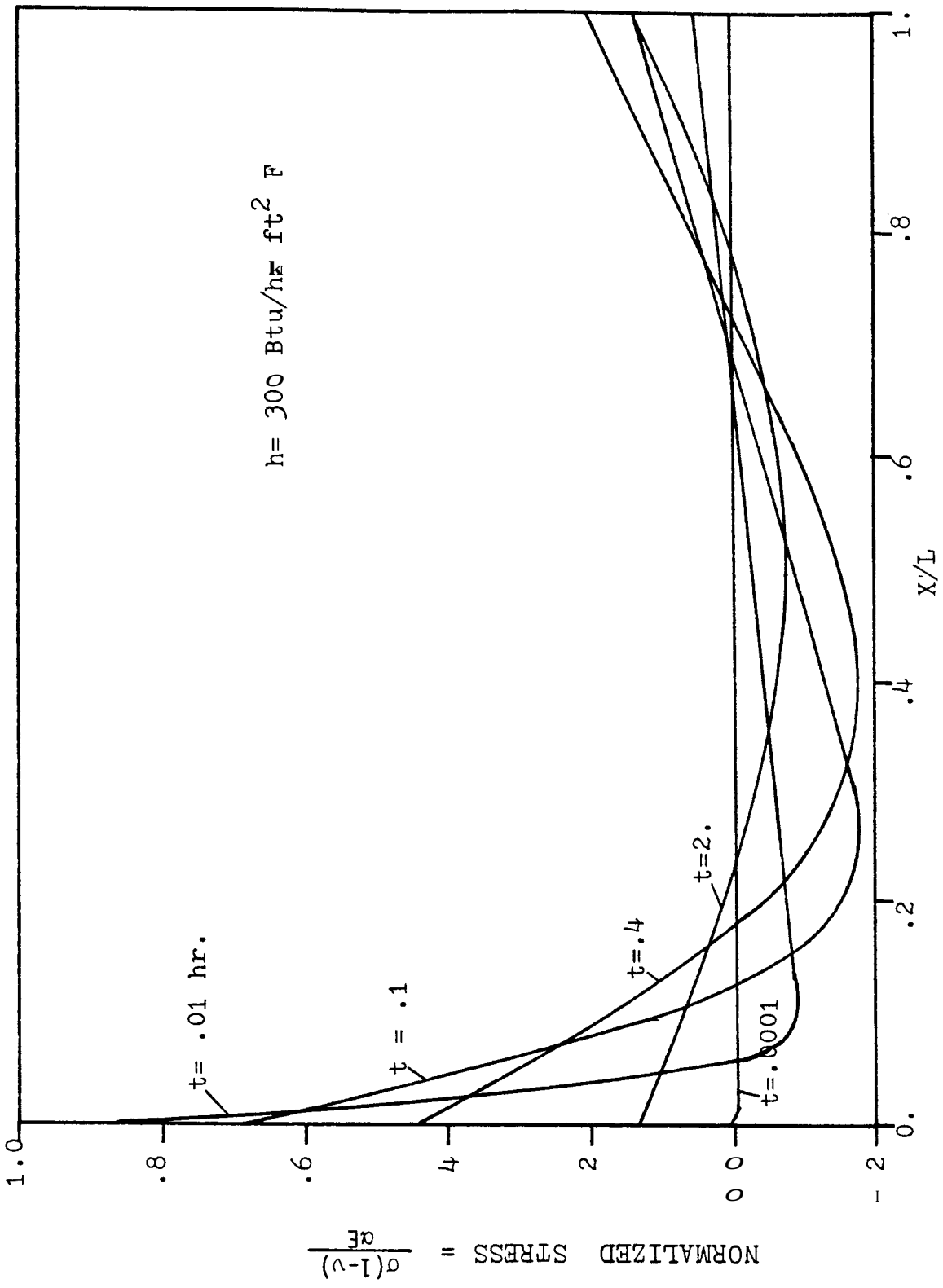

FIG. 3.8 Estimated Thermal Stress Distribution in Granite Block for h = 300 Btu/hr ft2 °F

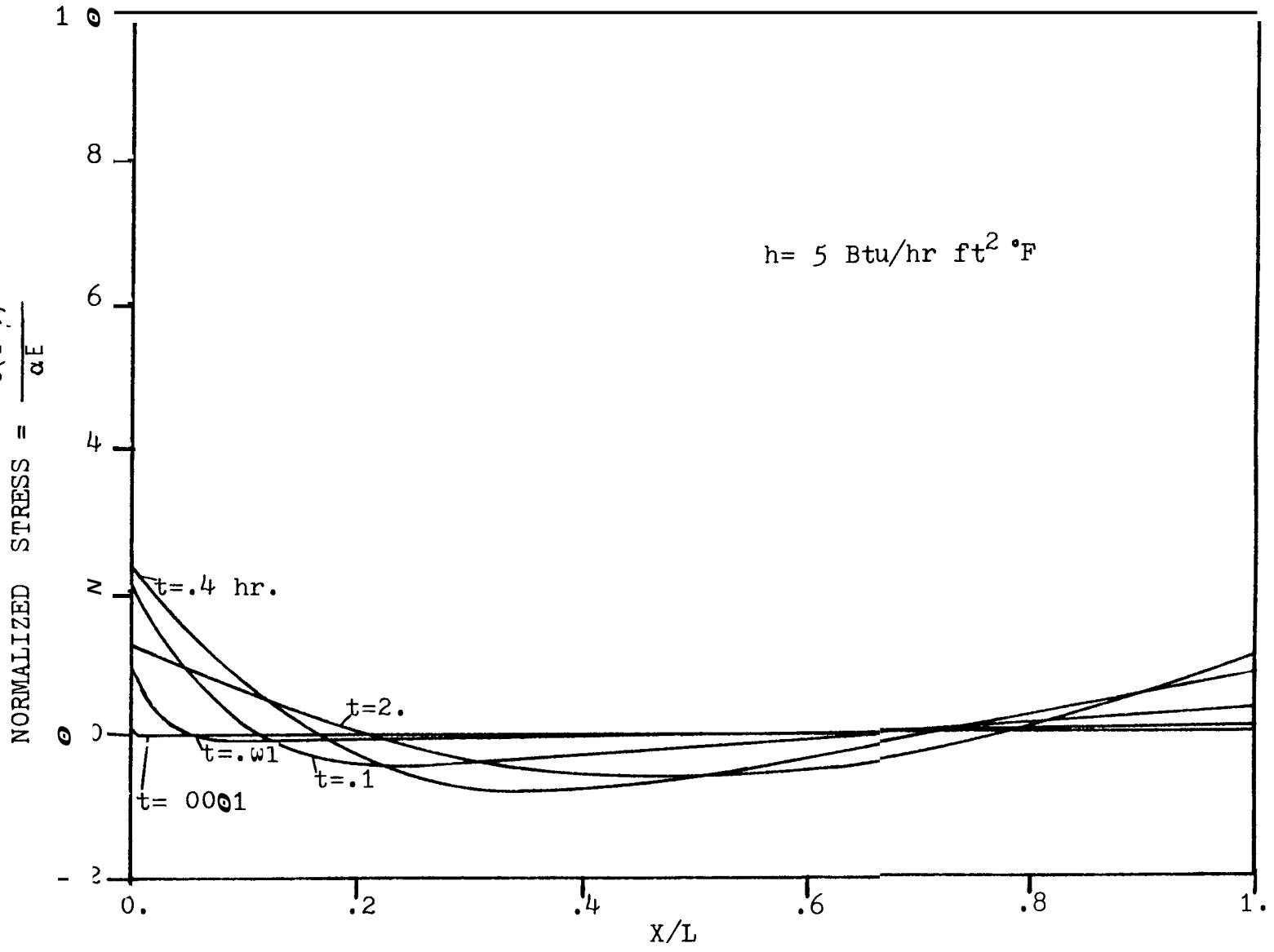

Fig. 3.9 Estimated Thermal Stress Distribution in Granite Block for h= 5 Btu/hr ft^2 °F

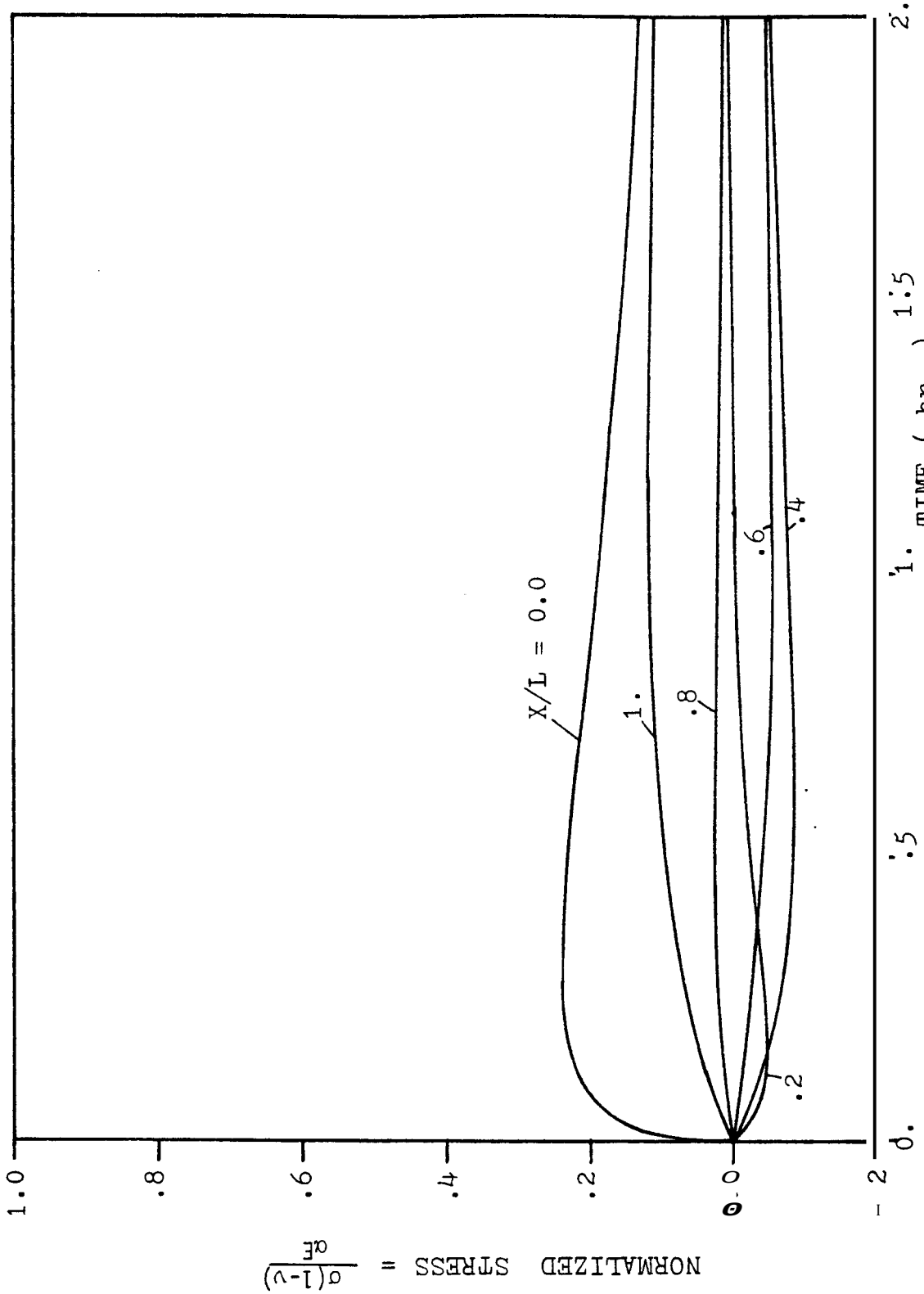

FIG. 3.10 Estimated Thermal Stress History in Granite Block for h = 5 Btu/hr ft^2 °F

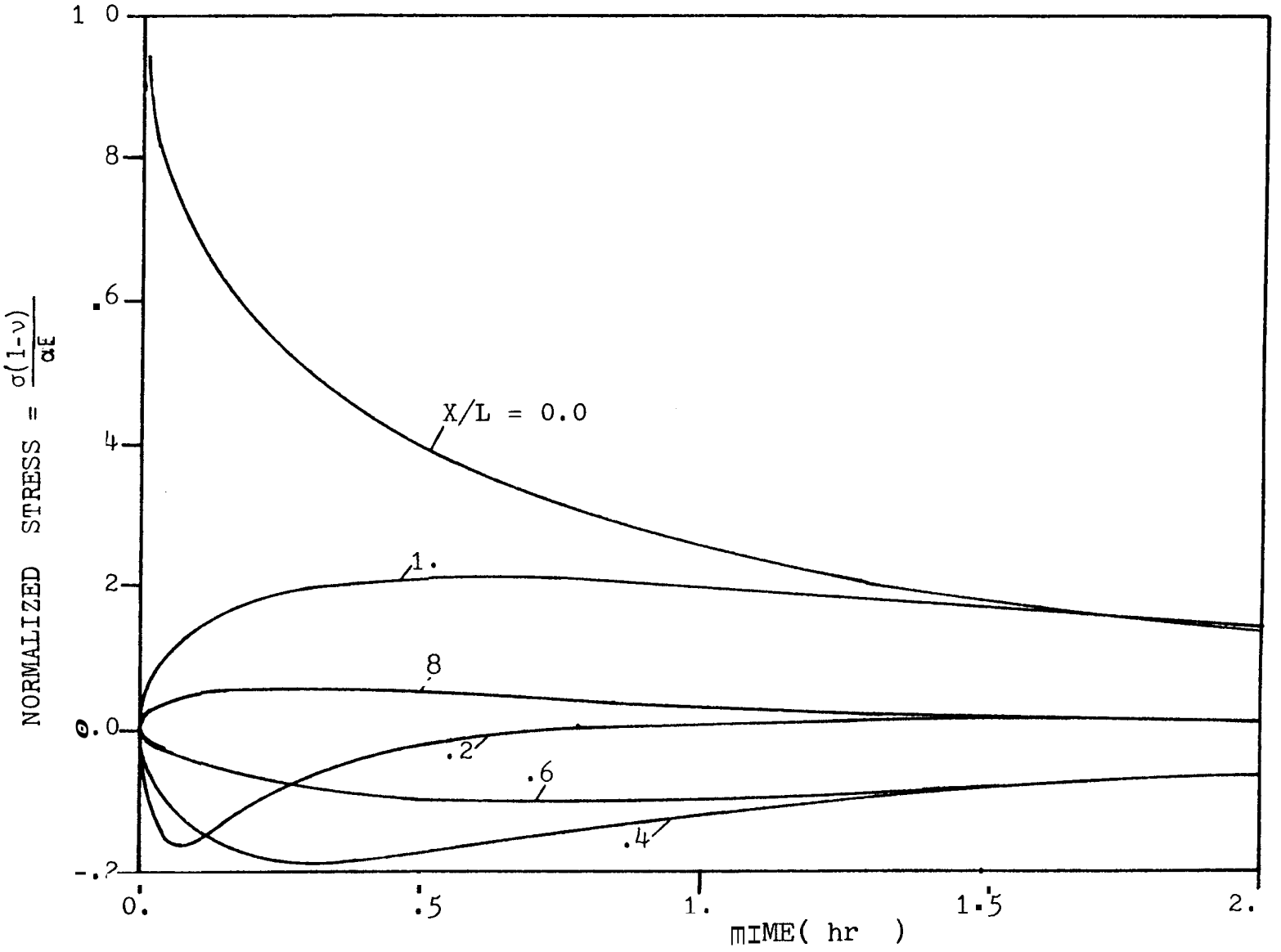

FIG 3 11 Estimated Thermal Stress History in Granite Block for h = 300 Btu/hr ft^2 °F

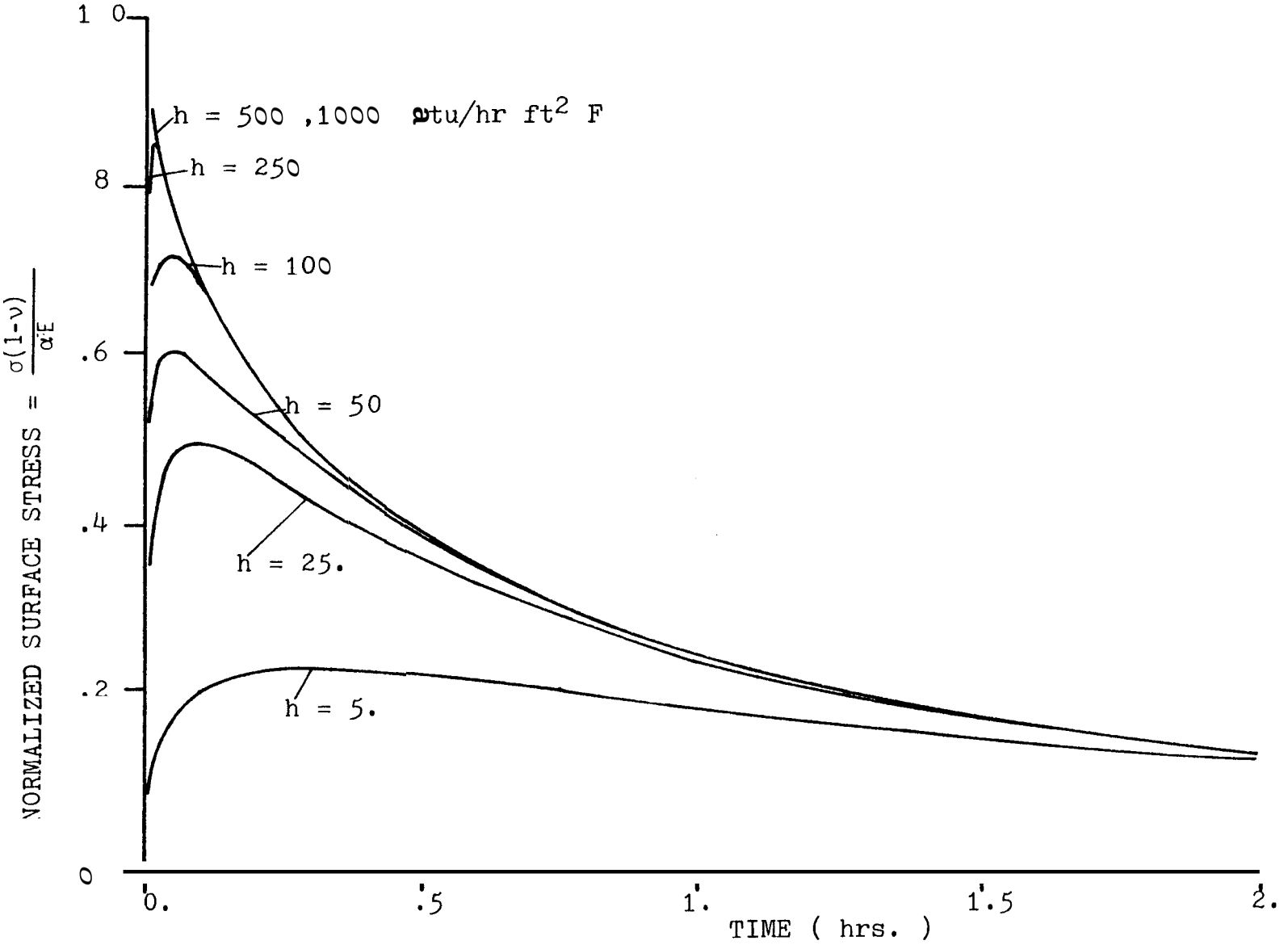

FIG 3 12 Estimated Surface Thermal Stress Variation in Granite Block

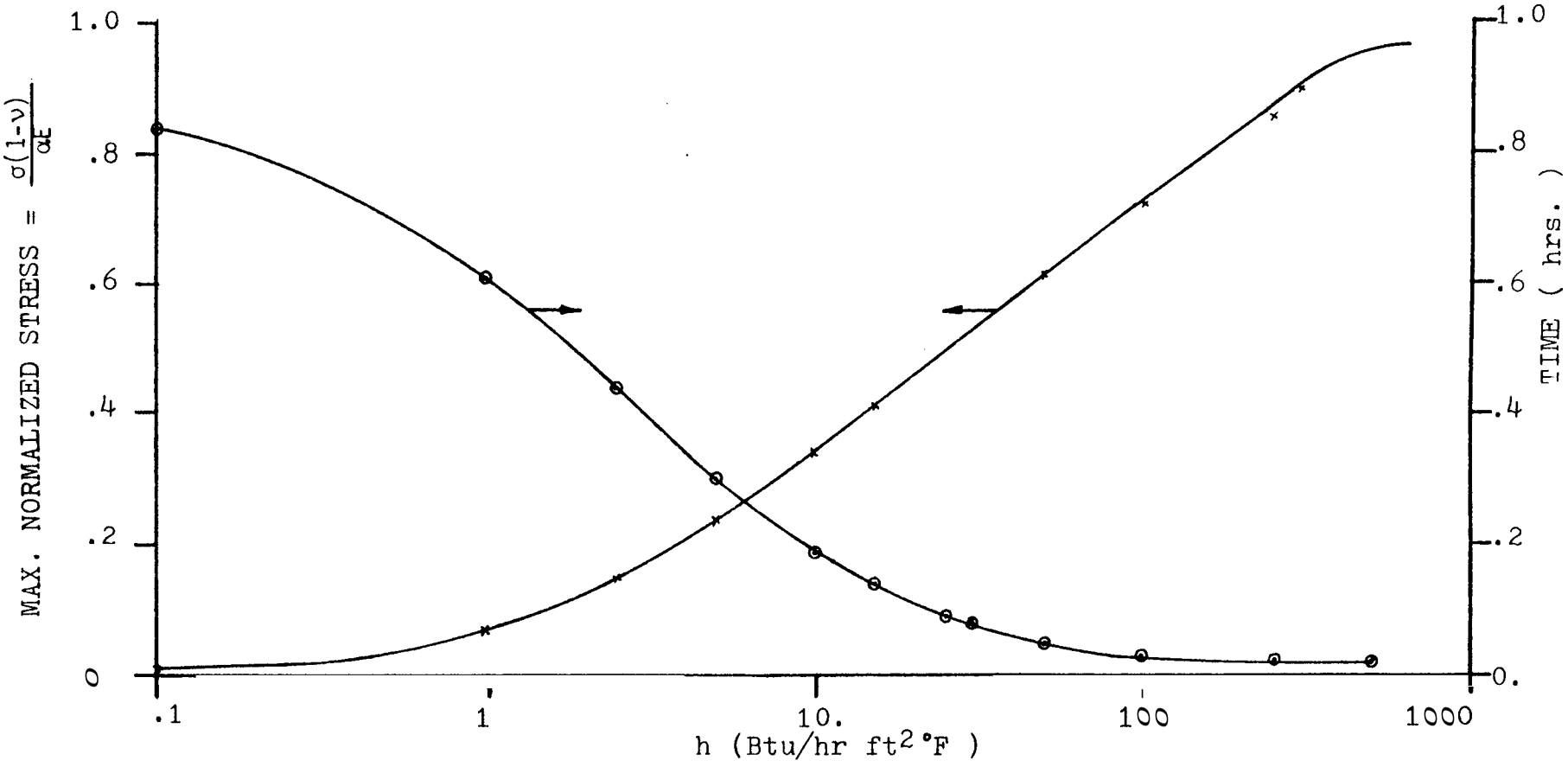

Fig. 3.13 Maximum Thermal Stress vs. Time for various heat transfer coefficients in Granite Block

shows that the maximum tensile stresses developed is much larger for higher heat transfer rates because of the correspondingly higher thermal gradients. Maximum compressive stresses are not appreciably different in the two cases. One interesting observation is that the transition from tensile to compressive stress occurs at almost equal values of X in both cases, which implies that the area under tensile stress remains roughly the same regardless of the heat transfer rate considered.

Figures 3.10 and 3.11 illustrate the time dependence of stresses at various distances from the surface for h = 5.0 and h = 300.0 Btu/hr. ft^2 F. As may be seen, all the stresses rise to a peak and then decrease slowly to zero. Comparing the two cases, one can conclude that peak stresses at all cross-sections are higher in the case of h = 300.0. Moreover, the stresses at the quenching face reach a peak value instantaneously for h = 300.0, whereas it takes a finite time to reach a maximum value for h = 5.0.

Since the maximum tensile stresses always occur at the surface, the time dependence of these stresses is of special interest. Figure 3.12 shows this variation for a range of heat transfer coefficient values. As can be seen from these curves, surface stresses first peak and then fade. Moreover, curves with high h values peak far sooner than those with low h values. The curves for values of h greater than 300.0 give identical surface stresses because the temperature -'time distribution remains the same for those heat transfer coefficients. These facts are brought out more clearly in Figure 3.13, which shows the peak stress values at the surface together with the times at which these maximum stresses occur.

An evaluation of the results presented in Figures 3.8 - 3.13 shows that in the case of thermally stressed semi-infinite slab. the critical

stresses arise either on the quenched face or in a region just below the surface. Since the compressive strength of a brittle material is generally larger than its tensile strength, failure is most likely to occur due to tensile stresses. The experimental work discussed in the next chapter describes the effects of thermal stress on the granite specimen strength.

3.4 Determination of Surface Heat Transfer Coefficient (h)

The discussion of various parameters affecting the thermal shock behavior of a brittle material showed that the knowledge of heat transfer coefficient is important for evaluation of quenching tests. The average surface heat transfer coefficient for the water jet and the rock surface system used here was determined using transient heat flow analysis of a plate with negligible internal resistance and also by comparing the cooling curves at two locations in a granite specimen with the theoretical cooling curves for a semi-infinite solid.

3.4.1 Determination of h Using the Transient Technique

The transient temperature response of a heated plate, cooled by the impinging water jets, is used as a basis for the evaluation of the average heat transfer coefficient. The time history of the temperature is recorded. The resulting "time constant" is directly related to the thermal resistance which varies inversely with h. The analysis is based on the "one-lump capacitance" parameter method since the internal thermal resistance of the plate can be demonstrated to be negligible compared to the external thermal resistance between the surface of the plate and the water jets. Figure 3.14 describes the thermal circuit for a flat plate model. The rate of decrease of internal energy of the plate, $\dot{E}$, is given by the following equation:

$$-\dot{E} = -\rho C_p V \frac{dT}{dt} = -\bar{C} \frac{dT}{dt} \qquad (3.15)$$

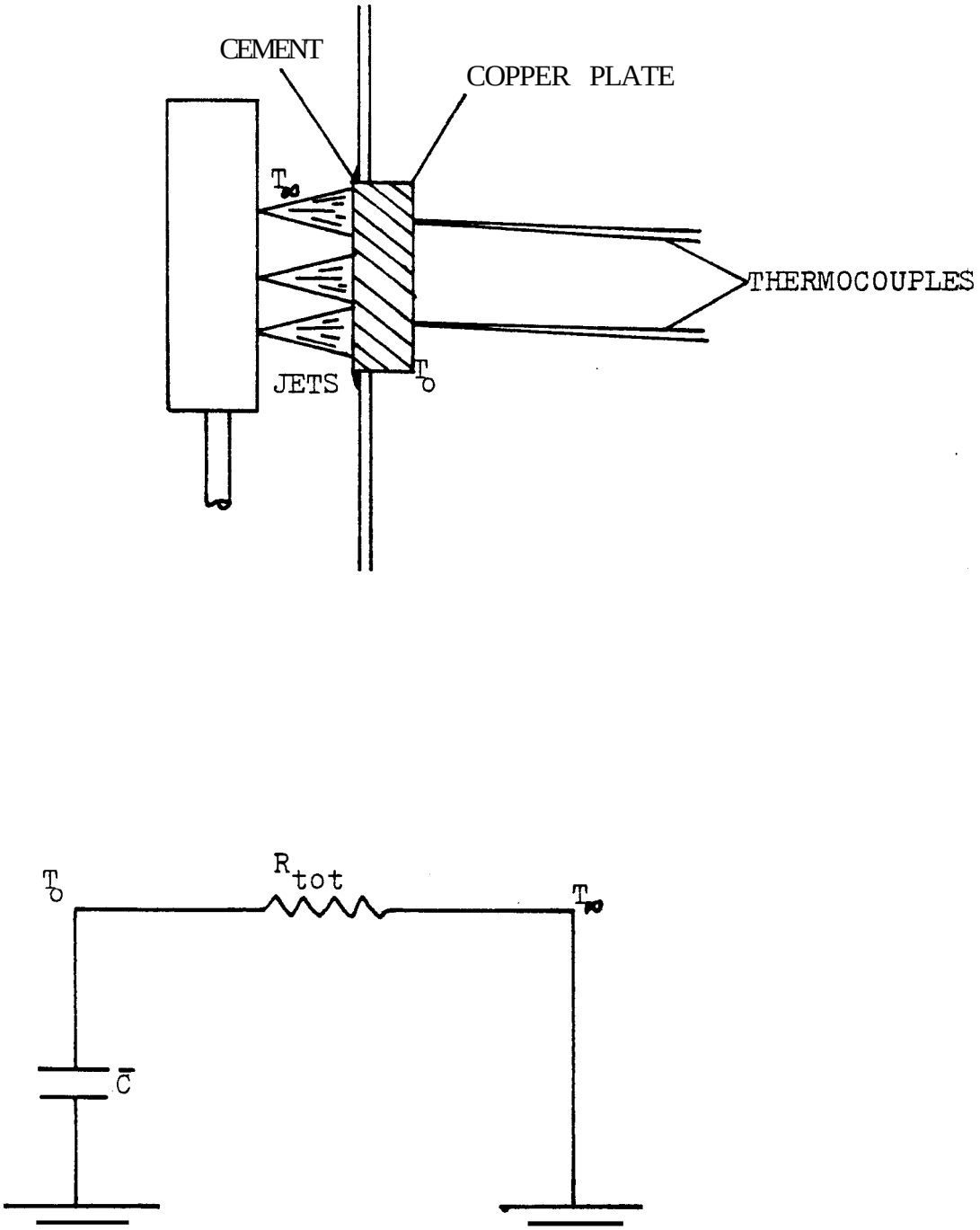

FIG. 3.14 Schematic of Copper Plate and Thermal Circuit Representation for Transient Technique

where: ρ = density of the plate material

C_p = specific heat of the plate material

V = volume of the plate

T = temperature of the plate

t = time

$\overline{C} = C_p V \rho$

The term $\overline{C}$ may be thought of as the capacitance of the plate. The rate of heat, q, transferred out of the body by convection is given by the equation

$$q = (hA)_{total} (T - T_\infty) \tag{3.16}$$

T_∞ = water jet temperature

A = surface heat transfer area

h = surface heat transfer coefficient

An energy balance yields

$$-E = q$$

or from Equations 3.15 and 3.16

$$-\overline{C} \frac{dT}{dt} = (hA)_{tot} (T - T_\infty) \tag{3.17}$$

Substitution of

$$\Theta = T - T_\infty, \quad \frac{dT}{dt} = \frac{d\Theta}{dt} \tag{3.18}$$

yields

$$\frac{d\Theta}{dT} + \frac{(hA)_{tot}}{\overline{C}} \cdot \Theta = 0 \tag{3.19}$$

The initial condition is

$$\Theta = \Theta_0 \qquad \text{at } t = 0$$

and the solution to Equation 3.19 is

$$\frac{\Theta}{\Theta_o} = - e^{- \frac{(hA)_{tot}}{\overline{C}} \cdot t} \qquad (3.20)$$

A plot of $\ln (\Theta/\Theta_o)$ versus t obtained from the test data should yield a straight line with the slope given by

$$m = \frac{(hA)_{tot}}{\overline{C}} \qquad (3.21)$$

A copper plate was used for the transient experiments. The relative importance of the thermal resistance within the plate can be written in dimensionless form as $\overline{h}\ L/k_s$, the Biot number, where $\overline{h}$ is the average unit surface conductance, L is the significant length dimension obtained by dividing the volume of the body by its surface area, and k_s is the thermal conductivity of the copper plate. In the copper plate, the error introduced by the assumption that the temperature at any instant is uniform will be less than 5 percent when the internal resistance is less than 10 percent, i.e., when $\overline{h}\ L/k_s < 0.1$ [22]. Using this condition and k_s = 216 Btu/hrftF and $\overline{h}$ = 500 Btu/hrft2F, the characteristic length is less than 0.5 in.

The copper plate used had a thickness of 0.5 inch. Several quenching runs were done for initial temperatures of 255°F and 370°F. The temperature history recorded showed quite a variation since boiling occurred at the surface. The most reproducible temperature histories are listed in Table 3.1. The plot in Figure 3.15 gives a slope which yields a value of h = 357.0. A similar plot for T_o = 370°F gives h = 582 Btu/hrft^{2}F. Higher values in the latter case were due to more severe boiling at the surface. The values of h evaluated by the transient technique would be higher than the actual values since the analysis does not account for radiation and natural convective losses.

Table 3.1

TEMPERATURE HISTORY IN COPPER PLATE

Time (min.)	Temp. (F)	$T-T_\infty$ (F)	$-\ell n\ (T-T_\infty/T_0-)T$
0.0	255.0	185.0	0.0
0.4	187.5	117.5	0.45
0.8	110.0	40.0	1.53
1.2	83.0	13.0	2.65
1.4	75.0	5.0	3.61
2.0	72.5	2.5	4.3
2.4	70.0	0.0	m

Time (min.)	Temp. (F)	$T-T_\infty$ (F)	$-\ell n\ (T-T_\infty/T_0-T_\infty)$
0.0	370.0	368.0	0.0
0.4	260.0	178.0	0.72
0.8	135.0	53.0	1.94
1.2	95.0	13.0	3.34
1.4	85.0	3.0	4.80
2.0	82.0	0.0	m

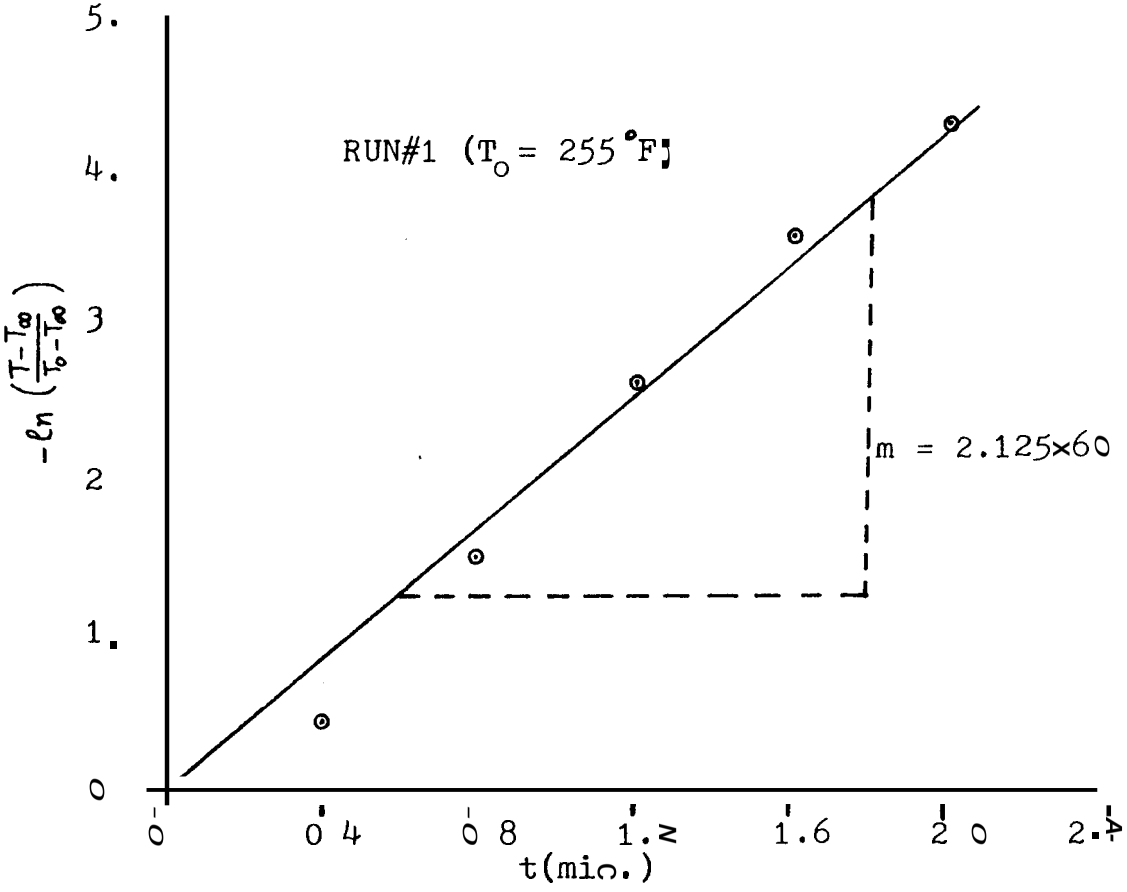

FIG. 3.15 Transient Temperature vs. Time Plot for Cu Plate

3.4.2 Determination of h Comparing Cooling Curves

Another method of determining average heat transfer coefficient for the quenching system is to compare the cooling curves at locations in the granite specimen with the theoretical cooling curves for arbitrarily assigned heat transfer coefficients. Temperature histories were recorded at locations X = 0.05 and X = 0.1 for an initial temperature of 440°F. A comparison of theoretical and experimentally-observed cooling curves at X = 0.05 is shown in Figure 3.16. It can be seen that the heat transfer coefficient is approximately 200 $Btu/hrft^2°F$. Dipping of the experimental cooling curve below the theoretical one during very early periods is attributed to boiling at the quenched face. Once the boiling is over, the experimental curve follows the theoretical ones more closely.

Comparison of cooling curves at X = 0.1 is shown in Figure 3.17. Again the heat transfer coefficient is about 200 $Btu/hrft^2°F$. The boiling effect is not observed since the location is further away from the quenched face. Since granite is a low conductive material, the boiling effect dies away in terms of its influence in the interior.

Once the heat transfer coefficient was determined approximately, another run was made for a half hour of quenching. The temperature history was recorded at X = 0.1 to check how well the condition of a semi-infinite solid is met experimentally. The temperature-time plot is shown in Figure 3.18 along with the experimental temperatures. There is an excellent agreement between the two cases thus ensuring that insulation of the specimen is very satisfactory.

From the experiments with the copper plate and the granite block, it appears that h for the water spray system will be on the order of 200 to 500 $Btu/hrft^2°F$. Due to the exploratory nature of the quenching experiments, more precise knowledge of h was not deemed necessary at this stage.

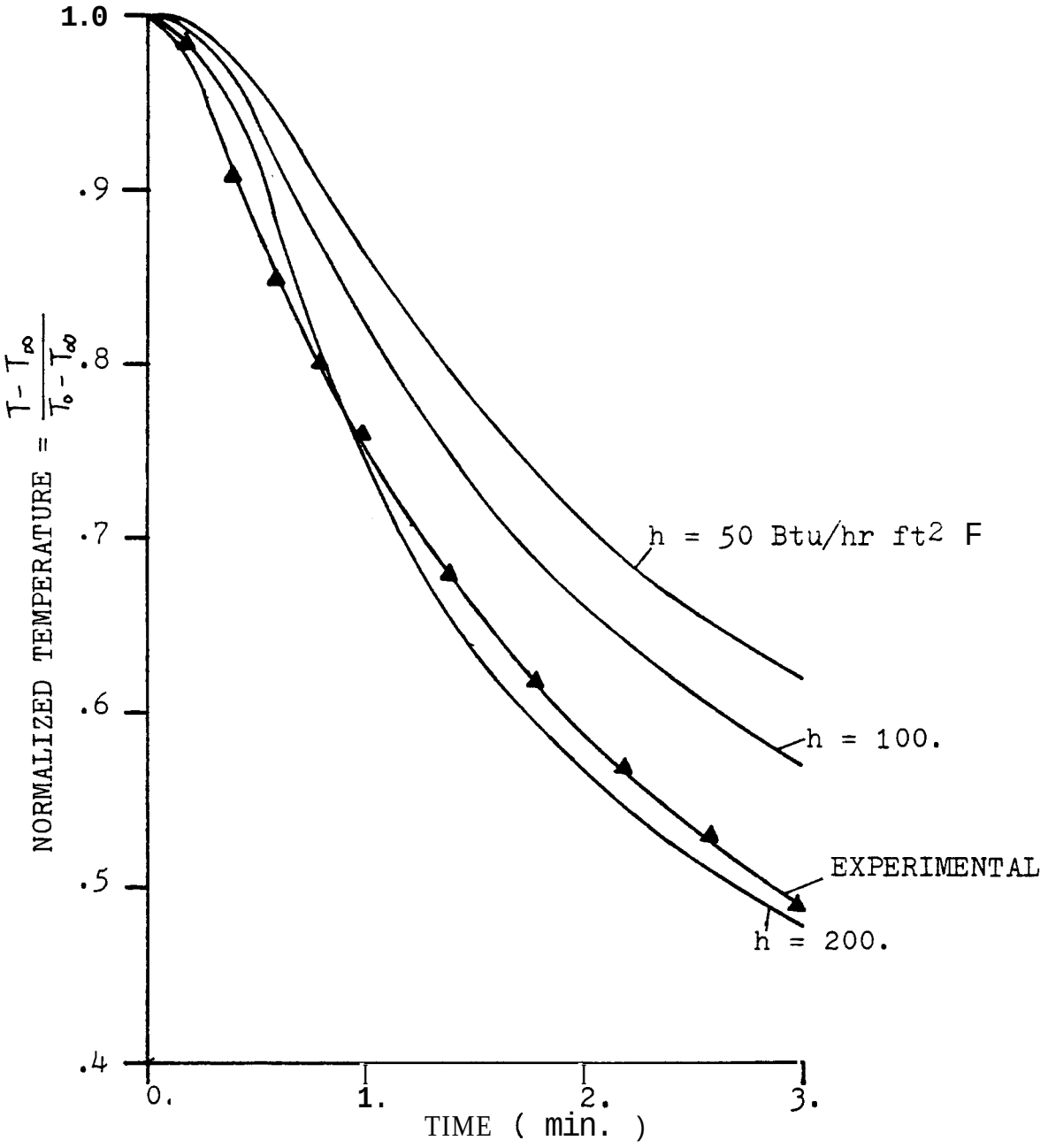

FIG. 3.16 Comparison of Cooling **Curves** at X = 0.05

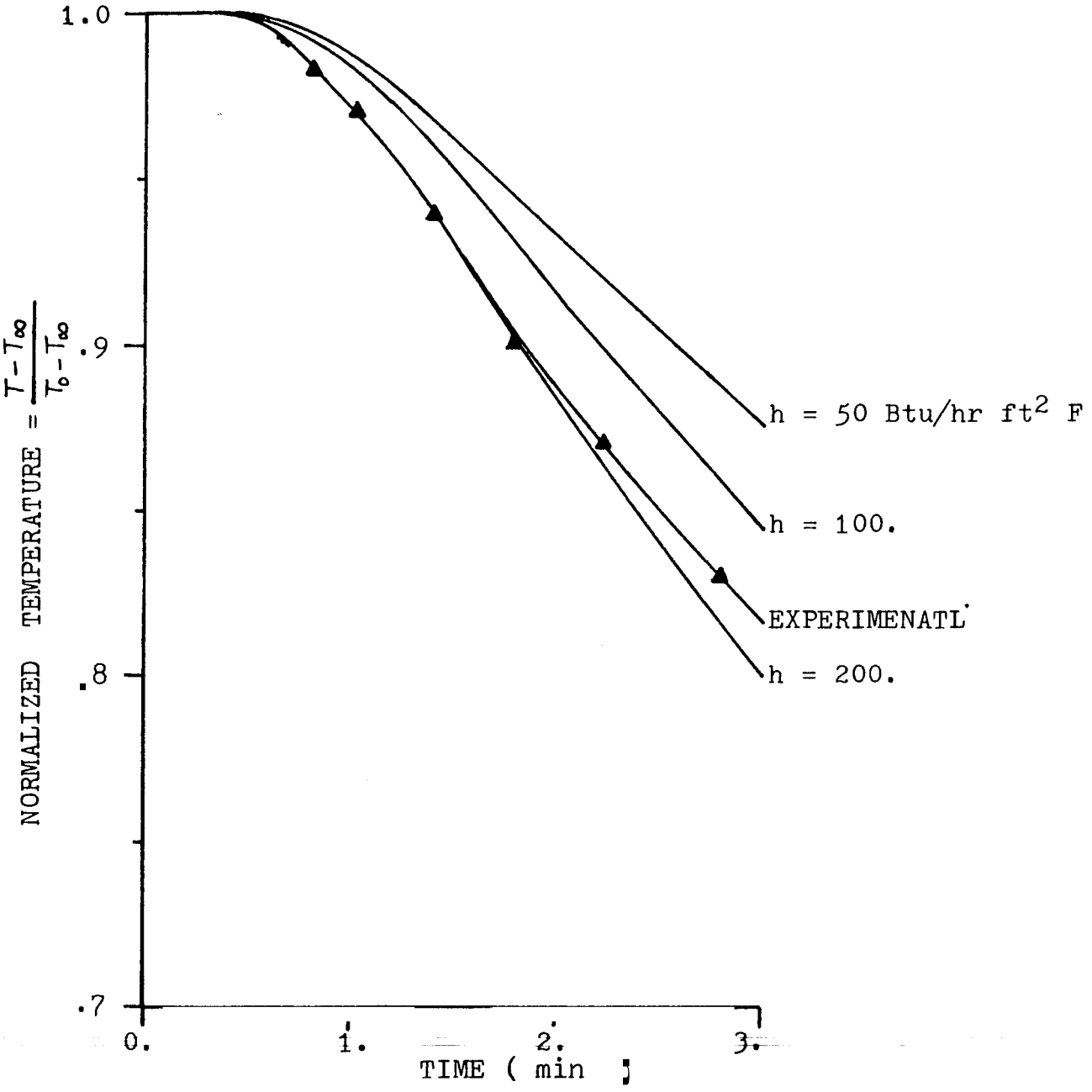

FIG. 3.17 Comparison of Cooling Curves at X = 0.1

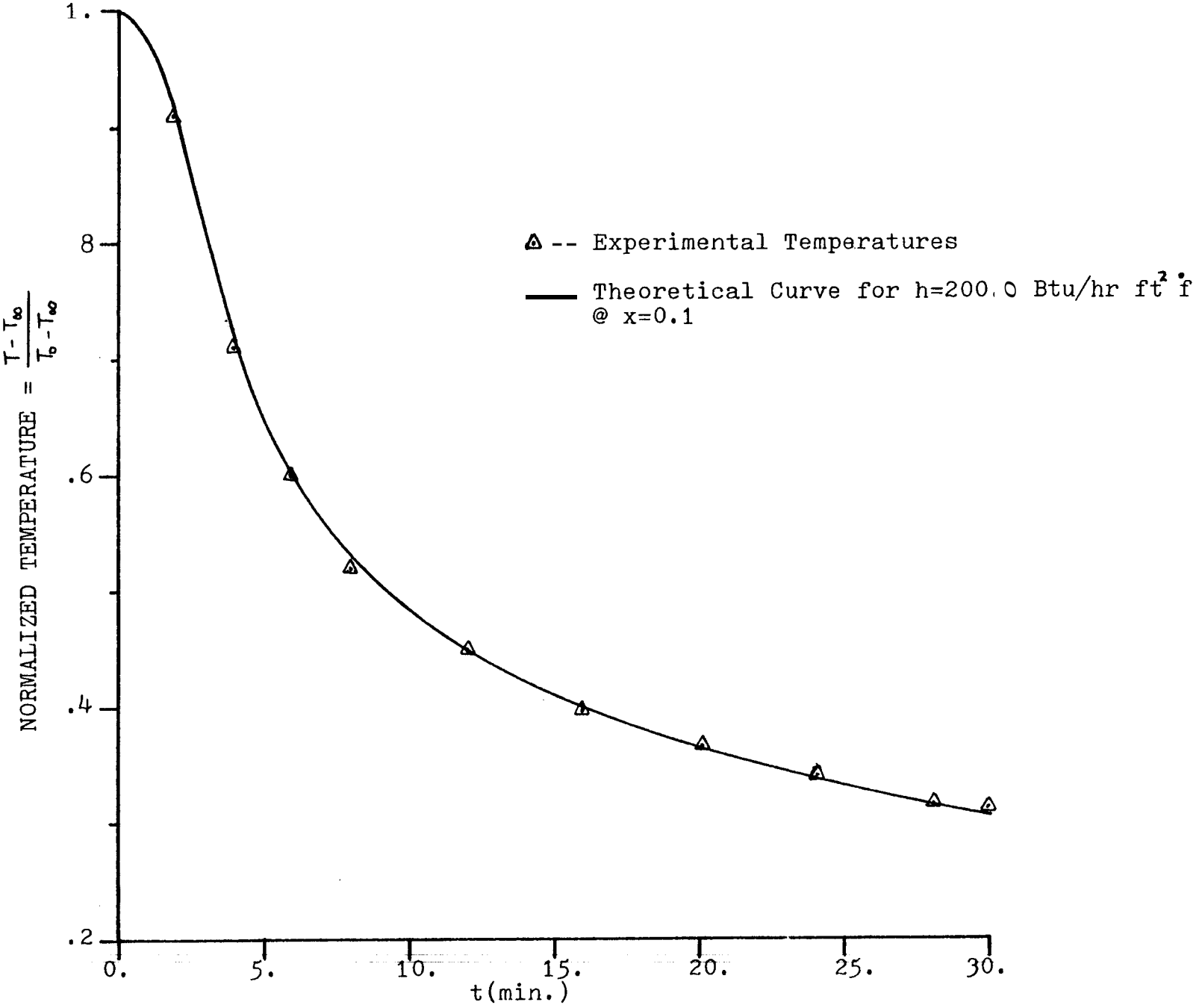

Fig. 3.18 Time-Temperature History at X = 0.1

3.5 Procedure to Determine Strength and Porosity Changes Due to Thermal Stressing

The experimental procedure used to investigate the post-thermal stress behavior of granite blocks is discussed in this section. Mechanical strength of thermally stressed specimens was evaluated using three point bending tests. The tests were carried out on a Universal Testing machine. Specimens for these tests were cut width-wise along the length of quenched and non-quenched blocks using a 1/32 in. diamond saw. The details of a typical bending test specimen are shown in Figure 3.19.

Porosity of the specimens was measured using two different methods, namely, the saturation method and Boyle's Law Porisimeter. An accurate determination of bulk volume of the specimen is important for porosity measurements. A Bulk Volume Meter, as described below, was used for these measurements.

The Bulk Volume Meter is based on displacement of a liquid by the specimen where the amount of displacement is measured in an inclined, calibrated tube with a suitable scale (Figure 3.20). The core sample is submerged under mercury in an adjacent connected chamber. The liquid displaced by the core is mercury but the liquid measured in the inclined tube is a hydrocarbon with low vapor pressure. The instrument is Calibrated by using cylinders of stainless steel instead of the core. The dimensions of the solids are measured with vernier calipers and a plot of volume versus scale reading is prepared. Only dry samples are used and submerged in the mercury with care being taken to prevent trapping air around the sample.

The apparatus used for porosity determination by saturation is diagrammed in Figure 3.21. The specimen is first cleaned and dried in an oven. After weighing, the clean, dry sample is placed in a vacuum

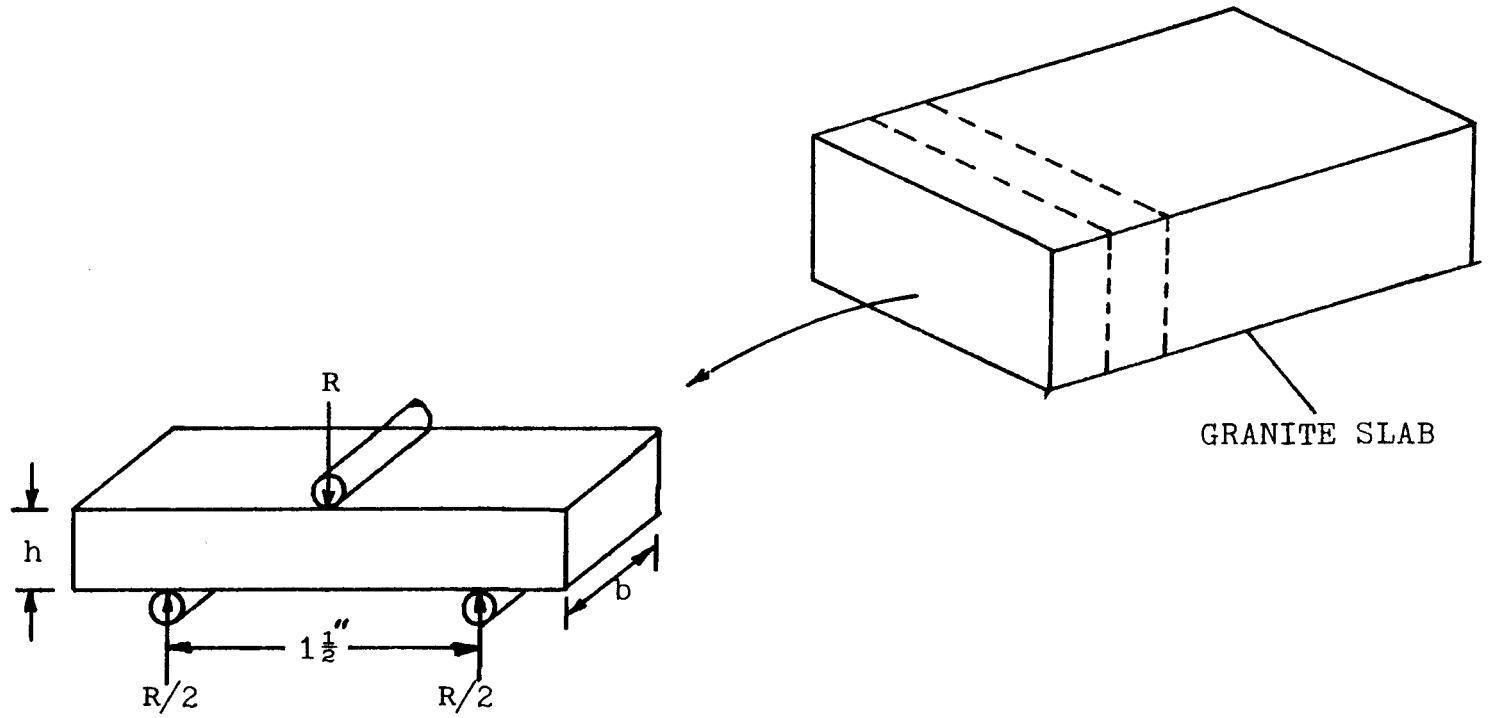

FIG. 3.19 Bending Test Specimen

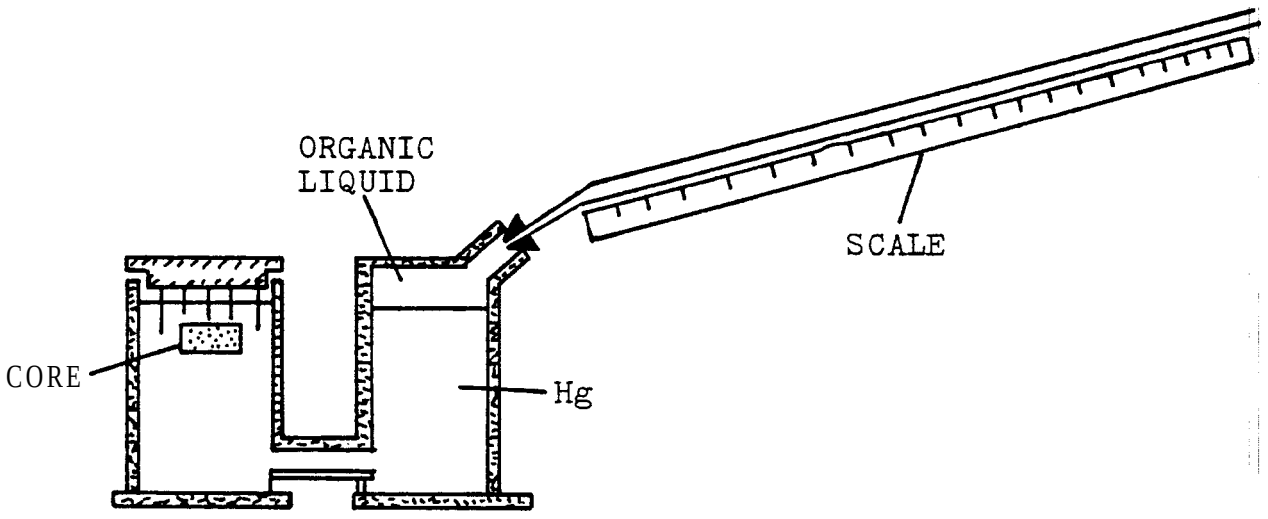

FIG. 3.20 **Bulk** Volume Meter

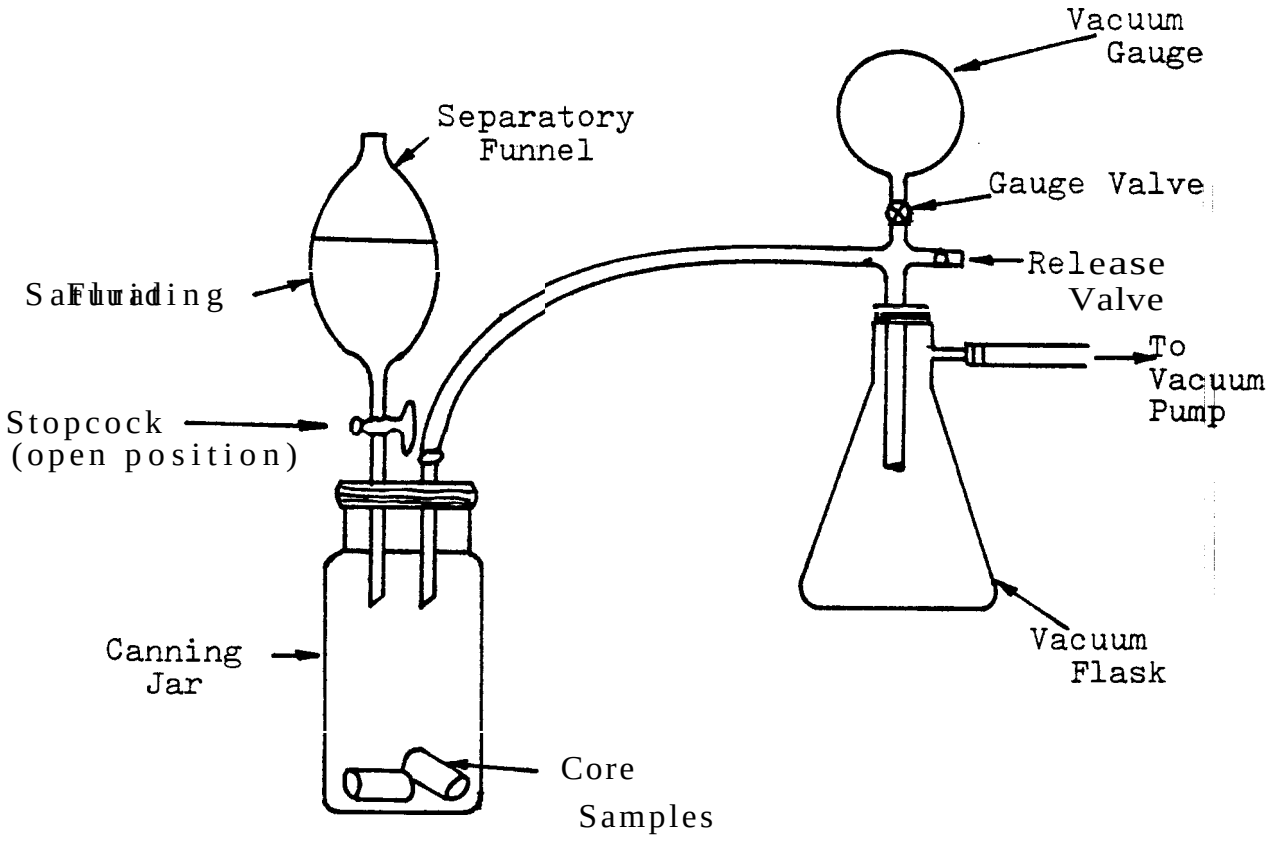

FIG. 3.21 Apparatus for saturating consolidated cores under vacuum

flask and all air evacuated. The saturation fluid (toluene) is admitted through a separatory funnel. When the saturation is complete, the sample is weighed. The porosity, ϕ, is determined from the relation:

$$\phi = \frac{W_{wet} - W_{dry}}{\rho V_b} \qquad (3.22)$$

where W_{wet} and W_{dry} are the weights in air of the wet and dry samples, ρ is the density of the saturating fluid, and V_b is the bulk volume of the core sample.

Boyle's Law Porisimeter, also used to determine porosity, measures the volume occupied by the grains and this subtracted from total or bulk volume gives pore volume. The grain volume is determined by applying Boyle's Law. The method and the instrument used here are due to the U.S. Bureau of Mines. The basic principles underlying the method are described below.

Consider an initial volume of gas, V_1, and an initial pressure, P_1. If this gas is allowed to expand isothermally so that there is an increase of volume, V_2, at a second pressure, P_2, then:

$$P_1V_1 = P_2(V_2 + V_1)$$

or

$$V_1 = P_2V_2/(P_1 - P_2) \qquad (3.23)$$

Now if we insert into the container, which originally held the initial volume of gas, a solid body of given volume and then repeat the gas expansion from the same initial pressure, P_1, to the same final pressure, P_2, we can again obtain the initial volume. However, this second initial gas volume, $V_{1,a}$, differs from the first by the volume of the solid body or by the volume of the grains, V_a, that is:

$$V_a = V_1 - V_{1,a}$$

or

$$V_a = \frac{P_2}{(P_1 - P_2)} (V_2 - V_{2,a}) \qquad (3.24)$$

where $V_{2,a}$ is the second final volume, that is, the volume after expansion when the core is in the container. Porosity is calculated by the equation:

$$\phi = \frac{V_b - V_a}{V_b} \qquad (3.25)$$

where V_b is the bulk volume of the sample. As seen from Equation **3.24,** merely a change of volume rather than an absolute volume is necessary if the same initial and final pressures are used for both measurements.

The instrument used for the determination of these volumes is shown schematically in Figure 3.22. The core holder is closed by a screw arrangement and sealed with an O-ring. Both the core holder and gas burette have jackets (not shown) through which constant temperature water is circulated. The mercury leveling bulb is used in conjunction with the gas burette to measure the final gas volume. The water manometer serves as a sensitive detector for the adjustment of the leveling bulb. The three-way stopcock connects the left or volume regulating part of the system. The vacuum regulator maintains a constant absolute pressure when connected to an adequate vacuum line. The vacuum gage is merely a mercury column supported by the difference in pressure between that in the system and the barometric pressure.

The system is made isothermal by using a water thermostat and flowing water around the core holder and the gas burette for an hour. With core holder in place, the toggle valve is opened momentarily to ensure the core

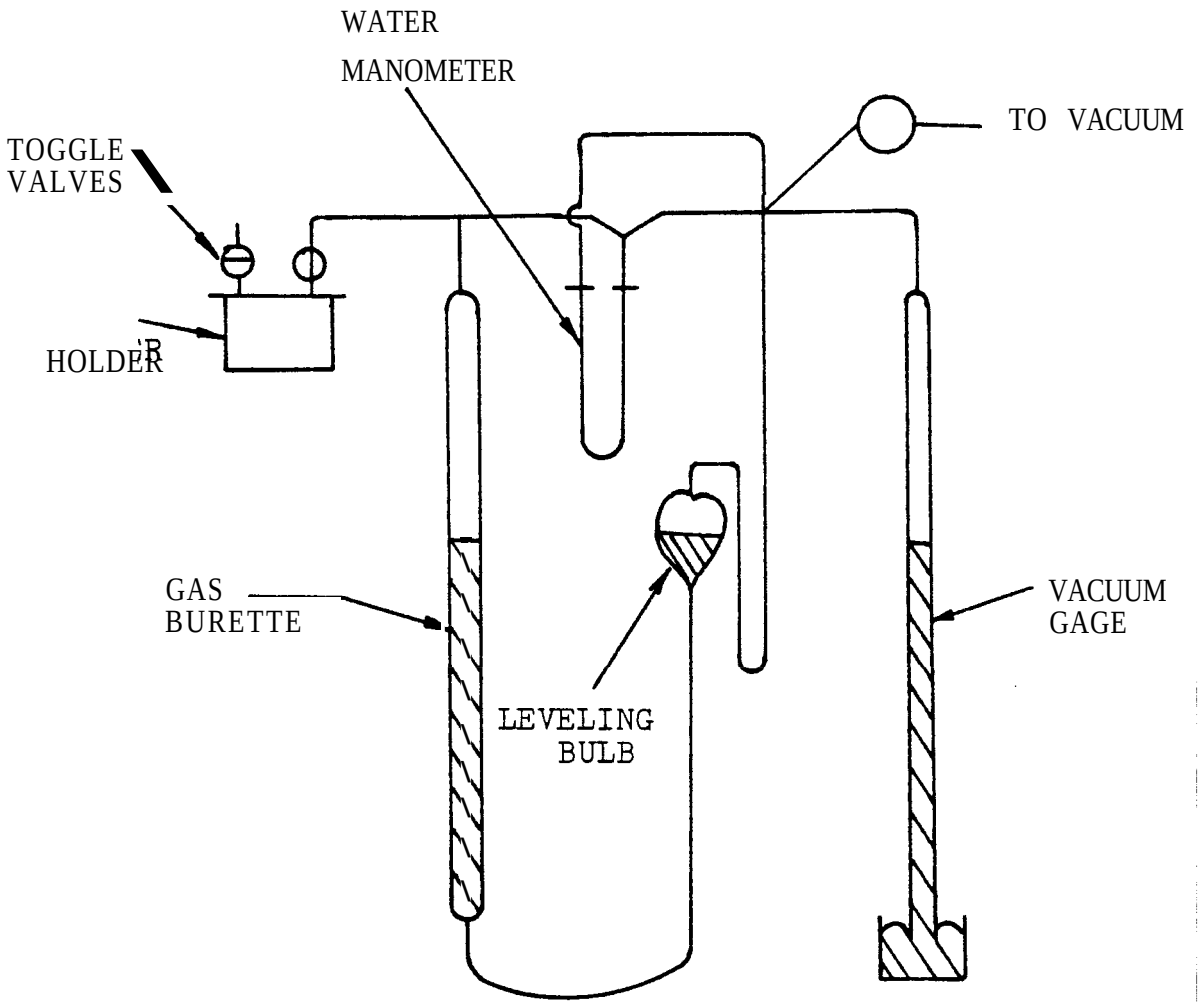

Fig. 3.22 Apparatus for **Boyle's** Law Porosity Measurements

holder is at atmospheric pressure. Then both toggle valves are closed to isolate the core holder. Vacuum is applied to the gas burette through the stopcock. When the desired vacuum is achieved, pressure and volume readings are taken, which are the two initial values for pressure and volume. The toggle valve connecting the core holder and gas burette is now opened slowly. Volume, V_2, and pressure, P_2, are measured after balancing the two levels of the water manometer. The above procedure is repeated with the sample in the core holder to find volume, $V_{2,a}$, and pressure, P_2. The grain volume of the sample can be calculated by using Equation (3.24) and porosity can be determined by knowing the bulk volume, V_b, of the sample.

4. TEST RESULTS

In order to explore the influence of thermal stressing, the strength and porosity of virgin samples were compared to values in samples removed from slabs which had been subjected to single and multiple quenches. The initial slab temperature was 450°F, which is typical or HDR rock temperatures. The temperature of tap water used for quenching was approximately 70°F. The quenching severity was that for which the values of surface heat transfer coefficient, h, were determined as described previously in section 3.4. In predicting temperature-time and thermal stress behavior a value of $h \simeq 300$ Btu/hrft^2°F was assumed, which is representative of the range of values determined experimentally and typical of values found in HDR reservoirs.

Specimen slabs were taken from larger blocks of Sierra White granite which is fine grained, grayish white, muscovite-biotite obtained from Raymond Quarry (Raymond, California). The pertinent properties of the rock are listed below.

Density, lb/ft^3	ρ	164
Poisson's Ratio	ν	0.30
Tensile strength, ps	σ_T	1100
Shear modulus, 10^6 psi	μ	2.44
Specific heat, Btu/lb°F	C_p	0.22
Coefficient of thermal expansion, 10^{-6}/°F	α	4.12
Thermal conductivity, Btu/hrft°F	k_s	1.57

An approximate chemical analysis s 74 percent silica, 15 percent alumina, 2 percent iron oxides, 3 percent ime, 5 percent soda and potash, and 0.3 percent combined water.

4.1 Bending Strength Tests

Tensile strength of the quenched and non-quenched specimens were measured by loading to fracture in three point bending. Table 4.1 shows the bending strength of eight specimen cut from a virgin rock. The mean bending strength was 1,835 psi with a 15 percent coefficient of variation. The uniaxial tensile strength was quoted as 1,100 psi. Higher values of tensile strength measured in bending tests are probably due to the smaller volume of rock being subjected to maximum tension and thus a reduced chance of flaws being subjected to the higher stresses.

The bending strength of specimens taken from various positions along the length of the quenched rock are listed in Table 4.2 through Table 4.5. Tables 4.2 and 4.3 are for one cycle of quenching, while the other two are for five cycles of quenching. These results are plotted in Figure 4.1a along with the theoretical stress distribution (Figure 4.1b). As can be seen, there is a significant degradation in strength in the specimens taken from near the quenched face, where tensile thermal stress was higher than the fracture tensile strength. On the other hand, there is no loss of strength in specimens taken from regions of compressive stress (see Figure 4.1b). The reduction of strength is about one-half for one cycle of quenching and two-thirds for five cycles of quenching. Also, exposure of the specimens to elevated temperature alone does not appear to cause loss of post-quench strength.

Table 4.1

BENDING STRENGTH OF VIRGIN GRANITE SPECIMENS

Specimen No.	Location (x/L)	b (in)	h (in)	Fracture Load (R) lbs	Fracture σ (psi)
1	0.18	2.05	0.3	154	1878
2	0.31	1.45	0.25	71	1762
3	0.43	1.475	0.275	80	1613
4	0.51	0.85	0.30	80	2353
5	0.59	1.00	0.30	60	1600
6	0.77	1.97	0.25	90	1640
7	0.90	1.48	0.25	90	2189
8	1.0	1.20	0.25	48	1640

Table 4.2

BENDING STRENGTH OF SPECIMENS AFTER ONE QUENCH

Specimen No.	Location (x/L)	b (in)	h (in)	Fracture Load (R) lbs	Fracture σ (psi)
1	0.15	1.5	0.27	45	926
2	0.31	1.5	0.27	100	2057
3	0.46	1.5	0.26	90	1997
4	0.62	1.5	0.26	95	2108
5	0.77	1.5	0.25	90	2160
6	0.85	0.7	0.25	40	1396
7	1.0	1.5	0.25	70	1680

Table 4.3

BENDING STRENGTH OF SPECIMENS AFTER ONE QUENCH

Specimen No.	Location (x/L)	b (in)	h (in)	Fracture Load (R) lbs	Fracture σ (psi)
1	0.18	1.5	0.27	45	926
2	0.37	1.5	0.27	100	2057
3	0.55	1.5	0.26	90	1997
4	0.73	1.5	0.26	95	2108
5	0.92	1.5	0.25	90	2160
6	1.00	0.69	0.25	70	1680

Table 4.4

BENDING STRENGTH OF SPECIMENS AFTER FIVE QUENCHES

Specimen No.	Location (x/L)	b (in)	h (in)	Fracture Load (R) lbs	Fracture σ (psi)
1	0.14	1.47	0.27	30	630
2	0.29	1.46	0.27	100	2113
3	0.43	1.46	0.28	110	2162
4	0.57	1.48	0.29	100	1808
5	0.72	1.47	0.25	100	2449
6	0.86	1.44	0.27	130	2729
7	1.00	1.46	0.33	110	1556

Table 4.5

BENDING STRENGTH OF SPECIMENS AFTER FIVE QUENCHES

Specimen No.	Location (x/L)	b (in)	h (in)	Fracture Load (R) lbs	Fracture σ (psi)
1	0.16	1.5	0.30	50	830
2	0.31	1.44	0.30	110	1833
3	0.46	1.44	0.30	95	1652
4	0.61	1.44	0.30	1001	1760
5	0.76	1.44	0.30	95	1896
6	0.84	0.94	0.28	55	1683
7	1.0	1.375	0.60	60	1570

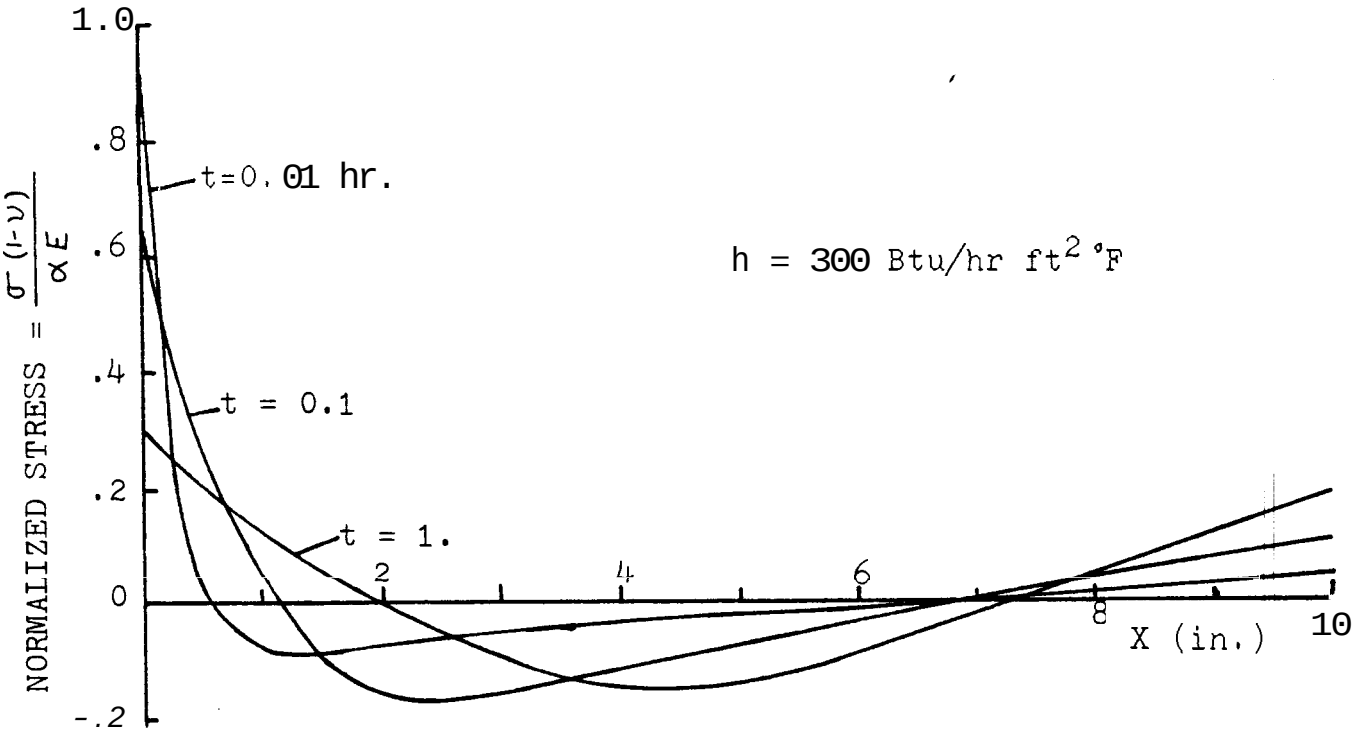

Fig. 4.1b Estimated Thermal Stress Distribution in Granite Block

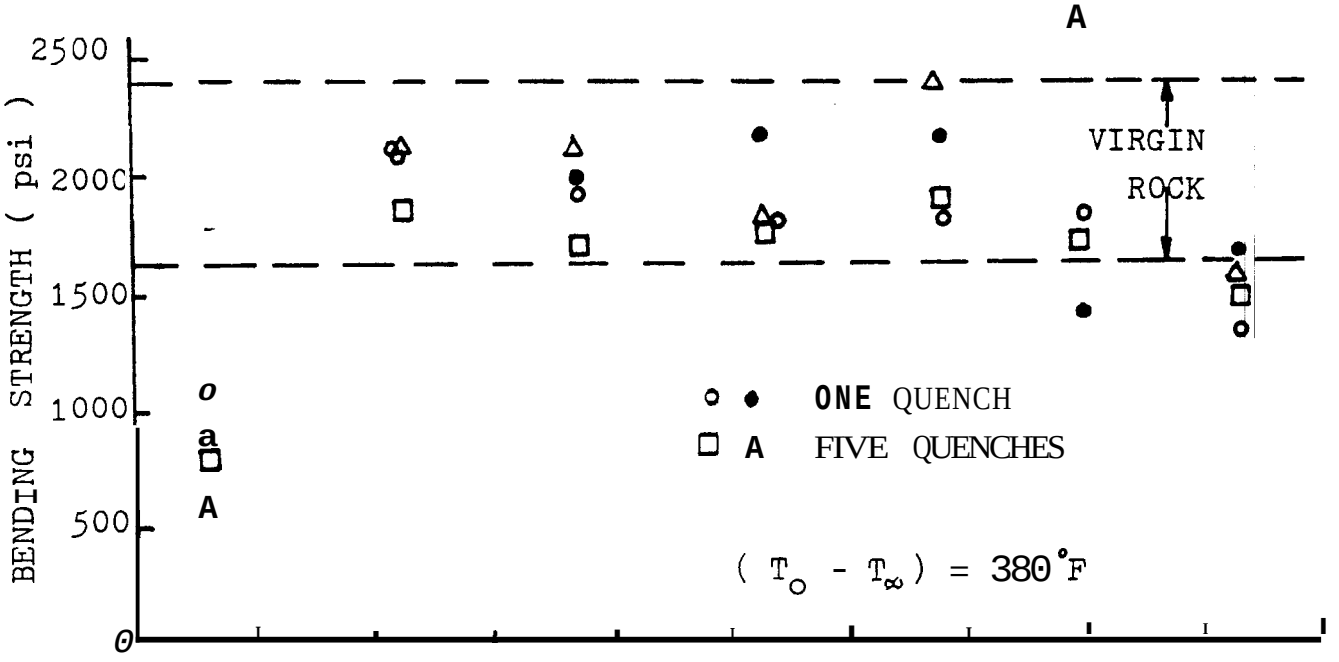

Fig. 4.1a Bending Strength of Specimens Taken From Block

4.2 Porosity Evaluation

Porosity was measured using both the saturation method and Boyle's Law Porisimeter (BLP). The measurements by BLP are not mentioned here since the results were not reproducible and there was a large variation even for virgin rock. The accuracy of the set up available in the laboratory was not enough to give correct estimates for low porosity rock. Porosity measurements done by the saturation method are given in Table 4.6. As can be seen, the porosity of an unquenched rock lies between 1.4 to 2 0. Porosity increases to 3.5 - 4.0 after one cycle of quenching and to 4.5 - 5.0 after five cycles of quenching.

4.3 Dye Penetrant Method

Direct observation of cracks was attempted by applying dye penetrant to one face of quenched and non-quenched specimens and a developer used to look at the micro cracks. It was seen that the quantity of dye fixed to the quenched specimens was much more than that for virgin rock. No macro cracks were observed. It showed that there might be micro cracks although it did not provide any quantitative evaluation of them. When dye was applied to one face of quenched specimens, it seeped through to the other side much faster than in ones which were heated and cooled slowly in the air. Also, dye either did not seep through or took a very long time to seep in a virgin rock. These observations showed qualitatively that quenching increased the porosity of the rock, perhaps due to micro crack formation.

Table 4.6

POROSITY MEASUREMENT BY SATURATION METHOD

Virgin Rock

Sample No.	W_{dry} (gross) (gms.)	$(W_{wet}-W_{dry})$ (gms.)	V_b(cc)	ϕ(%)
1	23.8930	0.1372	9.42	1.8
2	25.0170	0.1592	9.83	2.0
3	23.2983	0.1121	9.13	1.5
4	28.4071	0.1313	11.07	1.5
5	26.3138	0.1626	10.39	1.9
6	30.5044	0.1446	11.86	1.5
7	22.6118	0.1022	8.96	1.4

Quenched Rock

	1	21.0310	0.2962	8.92	4.1
one cycle	2	26.3065	0.3285	11.1	3.7
	3	15.5385	0.2287	6.6	4.3
	4	25.3804	0.8943	10.69	4.4
five cycles	5	25.8080	0.4065	10.9	4.7
	6	18.6540	0.3619	7.9	5.7

5. DISCUSSION

This exploratory study has indicated that the strength of quenched granite can be considerably reduced in regions of tensile thermal stress. Moreover, a substantial increase in porosity was also observed in those regions.

According to Murphy's analysis [2], crack formation and growth with continued cooling will occur in HDR reservoirs when tensile thermal stress exceeds the compressive tectonic stress, assuming that the tensile strength of the rock is negligible. The increase in porosity due to tensile thermal stressing should promote the opportunities for rock to saturate and increase its pore pressure to hydrostatic levels. In turn, the hydrostatic stress should counteract the tectonic stress, thereby reducing the "effective" stress to be overcome by tensile thermal stress. This effect, along with the reduction in rock tensile strength, should increase the propensity for and rate of thermal crack propagation.

Absence of large cracking in these experiments was probably due to the small size of the specimens and to their lack of constraint by surrounding rock such as would be present in HDR reservoirs. The quenching set-up shown in Figure 5.1 could provide a simulation of constraint. Since only a small portion of the block would be quenched, the rest of the block would remain at its initial elevated temperature for relatively long periods of time. The stress developed in the quenched region should be a better approximation of the constrained case. The disadvantage of the set-up is that the analysis of transient temperature and thermal stress behavior would be more complicated than in the case tested here. Ideally, the block should also be subjected to externally applied compressive stress on its faces (except for the quenched face and the opposite one), but this would require a much more elaborate and costly experimental set-up.

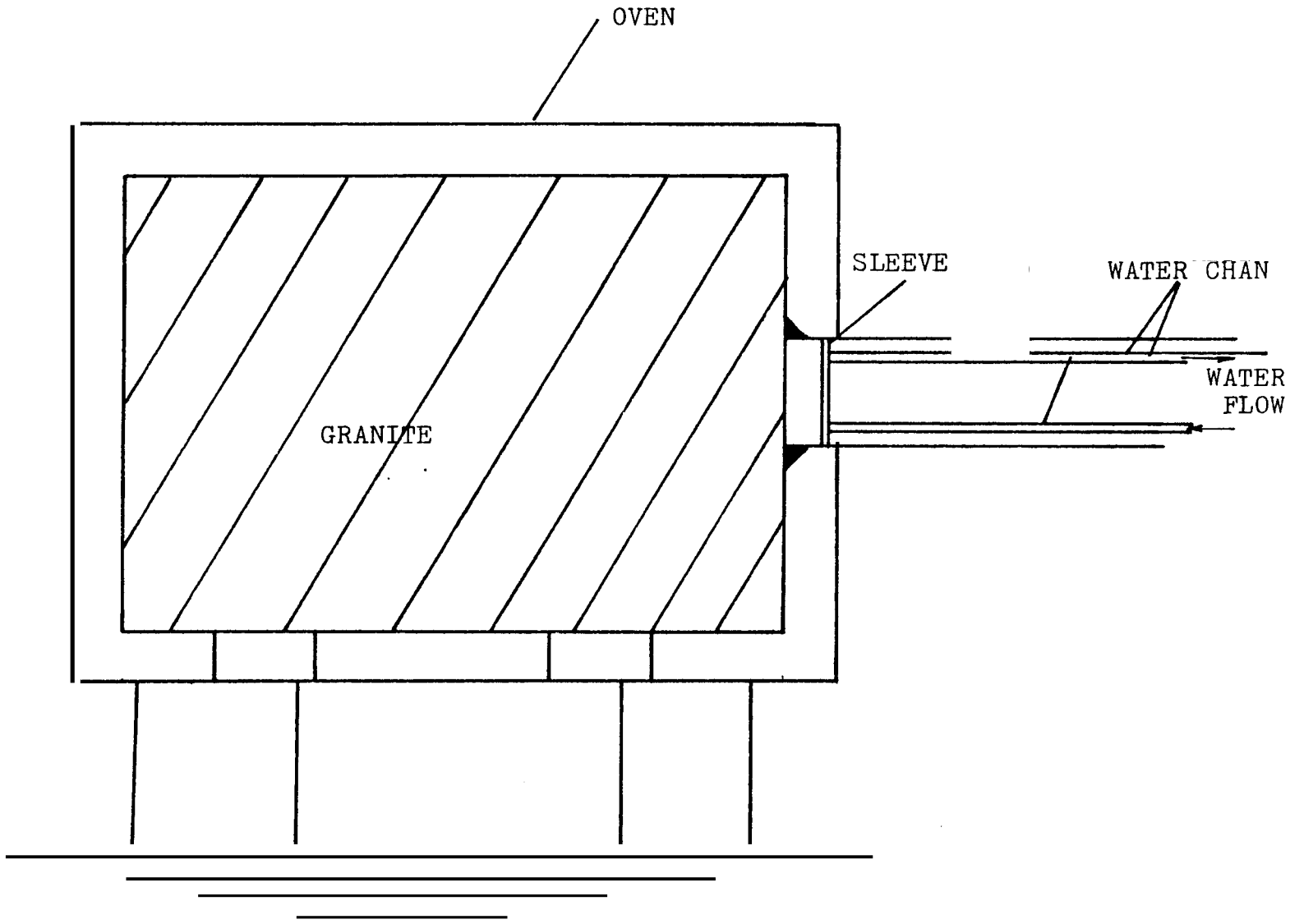

FIG. 5.1 Schematic of Experimental Setup to Better Simulate Stresses Under Geothermal Reservoir Conditions

The absence of macro cracking in the specimens used in these preliminary tests may also have been due to their relatively high initial porosity (≃ 2 percent). As discussed in Chapter 2, porosity in small specimens may act to arrest propagation of micro cracks which had been nucleated by tensile thermal stress. On the other hand, as noted previously, porosity may enhance growth of larger thermal cracks through introduction of hydrostatic pore pressure in actual reservoirs.

Future experiments on the influence of thermal stressing on rock behavior could also utilize the existing Stanford Geothermal Program reservoir model. By stacking large blocks of regular geometry in the pressure vessel, significant thermal stresses should be generated in blocks near the bottom of the vessel during "cold sweep" heat transfer experiments.

Other experiments could utilize blocks with flaws which have been cut into the surface to determine if the flaws would grow under thermal stressing. Such "pre-existing" flaws would provide a simulation of natural flaws which are likely to exist in HDR rock.

Future experiments should also check the influence of thermal stressing on the thermal conductivity of rock. It is conceivable that regions which experience significant tensile thermal stress may also experience a significant change in conductivity, thereby affecting the heat transfer to the cooling water. It is not apparent whether the conductivity is likely to increase or decrease or how significant the effect might be. This certainly seems worth investigating. If significant, changes in conductivity with thermal stressing could be incorporated into an analytic model for reservoir heat transfer.

6. CONCLUSIONS

(1) Tensile thermal stress produced by cooling conditions representative of HDR reservoirs caused a significant reduction in granite strength and a substantial increase in porosity.

(2) Strength reductions and porosity increases may favor formation and growth of larger thermal cracks in actual reservoirs by reducing local rock fracture toughness and allowing hydrostatic pore pressure to counteract tectonic compressive stress.

7. REFERENCES

1. White, D. F. and Williams, D. L., editors, "Assessment of Geothermal Resources of the United States--1975," U.S. Geological Survey Circular 726, 1975.
2. Murphy, H. D., "Thermal Stress Cracking and the Enhancement of Heat Extraction from Fractured Geothermal Reservoirs," Los Alamos Scientific Lab Report LA-7235-M, April 1978.
3. Nemat-Nasser, S., Kerr, L. M. and Parihar, K. S., "Unstable Growth of Thermally Induced Interacting Cracks in Brittle Solids," Int. J. of Solids and Structures, 14, p. 409, 1978.
4. Nernat-Nasser, S., "Stability of a System of Interacting Cracks," Letters Appl. Engrg. Sci., 16, p. 277, 1978.
5. Winkelman, A. and Schott, O., "Ueber Thermische Widerstaas-scoefficienten verschiedener Glaser in ihrer Abhangigkei von der Chemischen Zusammensetzung," Ann'n. Phys. Chem., 51, 1893-94, p. 730.
6. Lidman, W. G. and Bobrowsky, A. R., "Correlation of Physical Properties of Ceramic Materials with Resistance to Fracture by Thermal Shock," Tech. Note 1918, Natn. Advis. Comm. Aeronaut., Wash., 1949.
7. Cheng, C. M., "Resistance to Thermal Shock," J. Am. Rocket Soc., 21, Nov. 1951, p. 147.
8. Mason, S. S. and Smith, R. W., "Quantitative Evaluation of Thermal-Shock Resistance," Trans. Am. Soc. Mech. Engrs., 78, 1956, p. 533.
9. Marovelli, P. L., Chen, T. S., and Veith, K. F., "Thermal Fragmentation of Rock, "Proc. 7th Symp. Rock Mechanics, University Park, PA, 1965 (New York, AIME, 1965), Vol. 2, p. 252.
10. Hasselman, D. P. H., "Unified Theory of Thermal Shock Fracture Initiation and Crack Propagation in Brittle Ceramic," J. American Ceramic Society, 52, No. 11, p. 600.

11. Hasselman, D. P. H., "Griffith Criterion and Thermal Shock Resistance of Single-phase Versus Multiphase Brittle Ceramics," J. American Ceramic Society, 52, No. 5, p. 288.

12. Hasselman, D. P. H., "Crack Propagation Under Constant Deformation and Thermal Stress Fracture," Int. J. of Fracture Mechanics, 7, No. 2, June 1971, p. 157.

13. Davidge, R. W. and Tappin, G., "Thermal Shock and Fracture in Ceramics," Trans. Brit. Ceramic Soc., 66 (8), p. 405, 1967.

14. Coble, R. L. and Kingesy, W. D., "Effect of Porosity on Thermal Stress Fracture," J. Am. Ceram. Soc., 38 [1], p. 33, 1955.

15. Parmelee, C. W. and Westman, A. E. R., "Effect of Thermal Shock on Transverse Strength of Fireclay Brick," J. Am. Ceram. Soc., 11 [12], p. 884, 1928.

16. Bartsch, Otto, "Impact Bending Strength of Ceramic Bodies and Glasses and Its Relationship to the Resistance to Thermal Shock of Fireclay Bodies," Ber. Dent. Keram. Gest., 18 [11], p. 465, 1937, Ceram. Abst., 17 [11], p. 254, 1938.

17. Kato, S. and Okuda, H. "Relations Among Porosity, Thermal Shock Resistivity, and Some Physical Constants of Porcelain," Nagoya Kogyo Gijutsu Shikensho Hokoku, 8 [5], p. 37, 1959, Ceram. Abstr., 1959, p. 287a.

18. Richardson, H. M., "Choice of Refractions of Linings of Blast Furnaces," pp. 135-40 in Transactions of the VIIth International Ceramic Conference, London, 1960; Ceram. Abst., 1962, p. 2048.

19. Gupta, T. K. "Microstructural Dependence of Fracture in Alumina Subjected to Thermal Shock," Science of Ceramics, 1973, Vol. 7, p. 73.

20. Chyung, C. K., et al., "Electron Miscroscopy and Structural Materials, edited by G. Thomas, R. M. Fulreth and R. M. Fisher, Univ. of California Press, Berkeley and Los Angeles, CA, p. 1167, 1972.

21. Boley, B. A. and Weiner, J. H, Theory of Thermal Stresses, John Wiley & Sons, Inc., 1962, p. 277.

22. Kreith, "Principles of Heat Transfer," International Textbook Co., Scranton, PA, 1962.

23. Weibull, W., Proc. Roy. Swedish Inst. Eng. Res., No. 151, 1939.

APPENDIX: Computer Program to Evaluate Transient Thermal Stresses

```
CCCCCC
C     THE PROGRAM CALCULATES TENPERATURE PROFILE FOR A
C     SEMI-INFINITE SOLID USING SIMPSON'S RULE OF
C     INTEGRATION. THERMAL STRESSES ARE ALSO EVALUATED
C     USING SINPSON'S  RULE OF INTEGRATION.
CCCCCC
C      TENPERATURE OF A SEMI-INFINITE SOLID SUBJECTED TO
C      THERMAL SHOCK
CCCCCC
       IMPLICIT REAL*8 (A-H,O-Z)
       DINENSION THETA(201),T(201),STRESS(201),THETA1(101)
      $,X1(101),SUM1(201),SUM2(201)
       X=0.0
       DELX=0.01
       M1=201
       N1=101
       N2=N1-2
  100  FORMAT(F10.5 )
CCCCCCC
C      AL = THERMAL DIFFUSIVITY
C      KS = THERMAL CONDUCTIVIYT OF THE GRANITE
C      PL = LENGTH OF THE GRANITE BLOCK
CCCCCCC
       AL=0.042
       KS=1 .57
       PL=10./12.
       DO 18 I=1,N1
       X1(I)=0.01*DFLOAT(I-1)
   18  CONTINUE
       K=0
   9   READ(5,100) H
       K=K+1
       BIOTN=H*PL/KS
       TAU1=AL*H*H/(KS*KS)
       DO 15 J=2,M1
       T(J)=0 .01*DFLOAT(J-1)
       DD=PL*PL/(4.0*AL*T(J))
       TAU=DSQRT(TAU1*T(J))
       D=DSQRT(DD)
       TAU2=TAU*TAU
       DO 25 I=1,N1
       DX=D*X1(I)
       Y=DX+TAU
       IF(Y.GT.12.)GO TO 24
       THETA1(I)=DERF(DX)+(DEXP(X1(I)*BIOTN+TAU2))*(1 .-DE
       GO TO 25
   24  THETA1(I)=DERF(DX)
   25  CONTINUE
       SUM1(J)=0 .0
       SUM2(J)=0.0
       DO 26 I=1,N2,2
       SUM1(J)=SUM1(J)+THETA1(I)+4.*THETA1(I+1)+THETA1(I+2)
       SUM2(J)=SUM2(J)+X1(I)*THETA1(I)+4.*X1(I+1)*THETA1(I+1
      $+X1(I+2)*THETA1(I+2)
   26  CONTINUE
       DX=D*X
       Y=DX+TAU
       IF(Y.GT.12.)  GO TO 4
       THETA(J)=DERF(DX)+(DEXP(X*BIOTN+TAU2))*(1.-DERF(Y))
       GO TO 35
```

```
  4   THETA(J)=DERF(DX)
CCCCCC
C     EVALUATION OF THERMAL STRESSES
CCCCCCC
  35  STRESS1J)=-(THETA(J)-(4.0-6.0*X)*SUM1(J)*DELX/3.0-
     $6.0*(2.*X-1.0)*SUM2(J)*DELX/3.0)
  15  CONTINUE
      DO 10 I=2,M1
      WRITE(10,101) T(I),STRESS(I)
  10  CONTINUE
      WRITE(10,200)
 200  FORMAT( 'JOIN')
 101  FORMAT(2X,F10.8,2X,F12.8)
      IF (K.NE.6) GO TO 9
      STOP
      END
$DATA
```